INFORMATION TO USERS

The most advanced technology has been used to photograph and reproduce this manuscript from the microfilm master. UMI films the text directly from the original or copy submitted. Thus, some thesis and dissertation copies are in typewriter face, while others may be from any type of computer printer.

The quality of this reproduction is dependent upon the quality of the copy submitted. Broken or indistinct print, colored or poor quality illustrations and photographs, print bleedthrough, substandard margins, and improper alignment can adversely affect reproduction.

In the unlikely event that the author did not send UMI a complete manuscript and there are missing pages, these will be noted. Also, if unauthorized copyright material had to be removed, a note will indicate the deletion.

Oversize materials (e.g., maps, drawings, charts) are reproduced by sectioning the original, beginning at the upper left-hand corner and continuing from left to right in equal sections with small overlaps. Each original is also photographed in one exposure and is included in reduced form at the back of the book. These are also available as one exposure on a standard 35mm slide or as a 17″ x 23″ black and white photographic print for an additional charge.

Photographs included in the original manuscript have been reproduced xerographically in this copy. Higher quality 6″ x 9″ black and white photographic prints are available for any photographs or illustrations appearing in this copy for an additional charge. Contact UMI directly to order.

Order Number 1336556

Quality assurance for the clinical ferromagnetic seeds project

Sinno, Rami Assem, M.S.

The University of Arizona, 1989

U·M·I

300 N. Zeeb Rd.
Ann Arbor, MI 48106

QUALITY ASSURANCE FOR THE

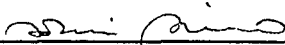CLINICAL FERROMAGNETIC SEEDS PROJECT

by

Rami Assem Sinno

_____

A Thesis Submitted to the Faculty of the

DEPARTMENT OF ELECTRICAL AND COMPUTER ENGINEERING

In Partial Fulfillment of the Requirements
For the Degree of

MASTER OF SCIENCE
WITH A MAJOR IN ELECTRICAL ENGINEERING

In the Graduate College

THE UNIVERSITY OF ARIZONA

1 9 8 9

STATEMENT BY AUTHOR

This thesis has been submitted in partial fulfillment of requirements for an advanced degree at The University of Arizona and is deposited in the University Library to be made available to borrowers under rules of the Library.

Brief quotations from this thesis are allowable without special permission, provided that accurate acknowledgment of source is made. Requests for permission for extended quotation from or reproduction of this manuscript in whole or in part may be granted by the head of the major department or the Dean of the Graduate College when his or her judgment the proposed use of the material is in the interest of scholarship. In all other instances, however, permission must be obtained from the author.
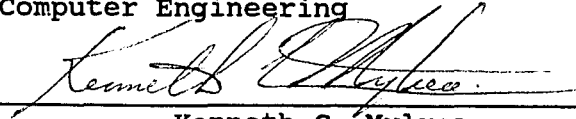
SIGNED: _____

APPROVAL BY THESIS DIRECTOR

This thesis has been approved on the date shown below:

_____   _____
Thomas C. Cetas   Date
Professor of Radiation Oncology
and Professor of Electrical and
Computer Engineering

_____   _____
Kenneth C. Mylrea   Date
Director, Clinical Engineering
Associate Professor of Electrical
and Computer Engineering

ACKNOWLEDGMENTS

I wish to express my sincere appreciation to my thesis director, Dr. Thomas C. Cetas for his most valuable guidance throughout the stages of the research and for the generous time and constructive criticism he gave to this study.

My deep appreciation and thanks go to Dr. Kenneth C. Mylrea and Dr. Randall K. Bahr for their helpful suggestions and for serving as members of the examining committee.

I give special thanks to fellow graduate students Jong Sheng Chen and Mohan Gopal for their helpful suggestions and practical assistance in all phases of the work.

TABLE OF CONTENTS

TABLE OF CONTENTS - <u>Continued</u>

LIST OF ILLUSTRATIONS

LIST OF ILLUSTRATIONS - <u>Continued</u>

LIST OF ILLUSTRATIONS - <u>Continued</u>

LIST OF TABLES

ABSTRACT

Surgically implanted thermoregulating ferromagnetic seeds as a mean of inducing hyperthermia in malignant tumors has been successfully introduced in a clinical environment at the University of Arizona. This work covers topics in quality assurance for the method on two levels. The first level deals with the magnetic induction system where magnetic and electric fields are measured. A discussion on safety levels for patients and treatment personnel is given, and an optically coupled probe for magnetic field measurements is described. The second level treats the electrical characteristics of the ferromagnetic seeds. Systems to measure the permeability and conductivity of the seeds are presented with some typical results. Finally, hysteresis power loss in a seed is measured and compared to losses due to eddy currents.

CHAPTER 1

INTRODUCTION

Cancer is responsible for over half a million deaths in the United States this year alone as reported by the Journal of the National Cancer Institute. Medicine provided different modalities for treating the disease, surgery, chemotherapy and radiotherapy are the two prominent ones. There has been a great interest recently in another method to conquer cancer using heat[22]. Indeed, tumor masses are more likely to be heated to higher temperatures at a given power level than normal tissues due to the frequently compromised vascularity of tumors. Hyperthermia by itself has proven to be useful in treating cancer, but even more effective is the combination of radiation therapy and hyperthermia.

In the Radiation Oncology Department of the University of Arizona numerous devices are currently in service for delivering controlled heat to areas of the body[2]. Among these devices, microwaves at 915 MHz are being used for certain surface lesions. The helix system operating near 80 MHz induces heat over a larger region such as the pelvis and is capable of whole body hyperthermia. The scanned, focussed ultrasound system allows the treatment of

both superficial and deep-seated tumors.

There are two major problems in the utilization of hyperthermia. These are directing heat only to the diseased area (except for the whole body hyperthermia), and controlling the tumor temperature. Both of these problems could be overcome by the use of the thermoregulating ferromagnetic seed modality.

The ferromagnetic implant heating system[1] is a localized heating system. It has been designed to be very compatible with interstitial brachytherapy[2], with the implants surgically placed in the specific volume to be heated.

A description of the technique is that a number of small ferromagnetic seeds (1cm long and 1mm in diameter) are introduced into a tumor at a density of about 1 seed per centimeter cube. For that, the patient is checked into the operating room where a surgeon implants a number of blind ended hollow plastic catheters in the tumor in a certain array. Usually the array allows for at least 1 cm spacing between any two catheter. The patient is allowed to recover and then brought to a treatment room where the ferromagnetic seeds in ribbon form are inserted inside the catheters. Thermometry probes are also used to monitor the tumor temperature. The patient is then placed in a coil producing a strong magnetic field at around 100 kHz. The ferromagnetic

seeds present in the magnetic field absorb the energy and heat up due to induced currents flowing on their surfaces (eddy currents). The seeds are oriented parallel to the axial magnetic field for efficient heating. They heat the tumor by thermal conduction. As a result, only the implanted volume absorbs energy, leaving the rest of the body at normal temperature. The treatment time is set for 30 minutes from the time the monitored temperature reach steady-state. At the end of the procedure, the ferromagnetic seeds are replaced by radioactive seeds and are kept in the patient for the prescribed period. A second heat immediately after the radiation therapy is usually administered.

The ferromagnetic seeds could be permanently implanted in the tissue when properly coated with biocompatible material. This will allow for another treatment without surgical procedure in case of a recurrent malignancy. At the present time, only temporary seeds are being used.

The material used for the seed is a nickel silicon alloy that changes from being ferromagnetic to being paramagnetic (Curie point) around 60 °C. This means that the absorbed power of the seed drops sharply as its temperature approaches its Curie point. Its temperature remains nearly constant even when the magnetic field strength is increased. Therefore temperature control is possible by the proper

choice of the Curie temperature for the seed.

Quality assurance for the ferromagnetic seed project encompasses a multitude of tasks. Among those are characterizing the magnetic field generating system (that is, the coils, the matching network and the generator), establishing methods of assuring the level of performance of this system, verify the accuracy of the thermometry system, determining the properties of the ferromagnetic implants, and establishing systems for routine measurements of seeds to be used clinically. Part of the effort involved was to ensure that the installation of the system in the new facility was carried out properly and that the hospital and Federal Communication Commission (FCC) frequency emission standards were met. The purpose of this thesis, then, is to provide a sound overall picture of the quality assurance of the system and procedures for routine clinical use. These are divided into two categories: the quality assurance of the magnetic induction system and the quality assurance of the seeds to be used in the clinic.

On the system basis, we are interested in magnetic field strength and electric field levels. The magnetic field is responsible for inducing eddy currents on the seeds that provides the heating. Therefore a strong magnetic field is required to provide sufficient power into the seeds. However, too strong of a field has adverse effects on the

body (for example by direct tissue heating). A magnetic field probe is presented in Chapter 3 and is used to scan the treatment room for fields generated by the three magnetic induction coils. The results of such mappings are presented in Chapter 5.

Electric fields can also have negative effect on the body. An instrument for electric field measurements is presented in Chapter 4 and the results are found in Chapter 5.

The safety levels for both electric and magnetic fields are discussed in Chapter 6.

Quality assurance at the seed level deals with measurement of the permeability of the seed, its conductivity and the amount of heat generated due to its hysteresis losses.

Permeability measurements are presented in Chapter 7. An automated device for that purpose is described together with some illustrative measurements.

Chapter 8 is about conductivity measurement. Here again a device built for that purpose is presented and data are given.

Finally, in Chapter 9, an equation for hysteresis losses are derived from a simple analytical instrument. Results of measurements carried out on a number of seeds are given.

CHAPTER 2

MAGNETIC INDUCTION SYSTEM

In this chapter, an overview of the magnetic induction system for the heating of the ferromagnetic seeds is be presented.

1. Components of the System

The magnetic induction heating system used for the ferromagnetic seeds technique is located in a shielded room as shown in Figure 1. The system consists of the following components:

1. An 8000 Watt variable frequency power generator, ENI model EGR-9600, with a frequency range from 8 kHz to 111 kHz,

2. A remote control panel, ENI model EGR-9600B,

3. A matching network designed and constructed by Dale Buechler[1] to match the induction coils to the generator, it consists of a parallel combination of capacitors and a matching transformer bathing in transformer oil (see Figure 2),

4. Three magnetic induction coils to provide the magnetic field for implant heating,

5. A cooling system to provide cooling to the matching
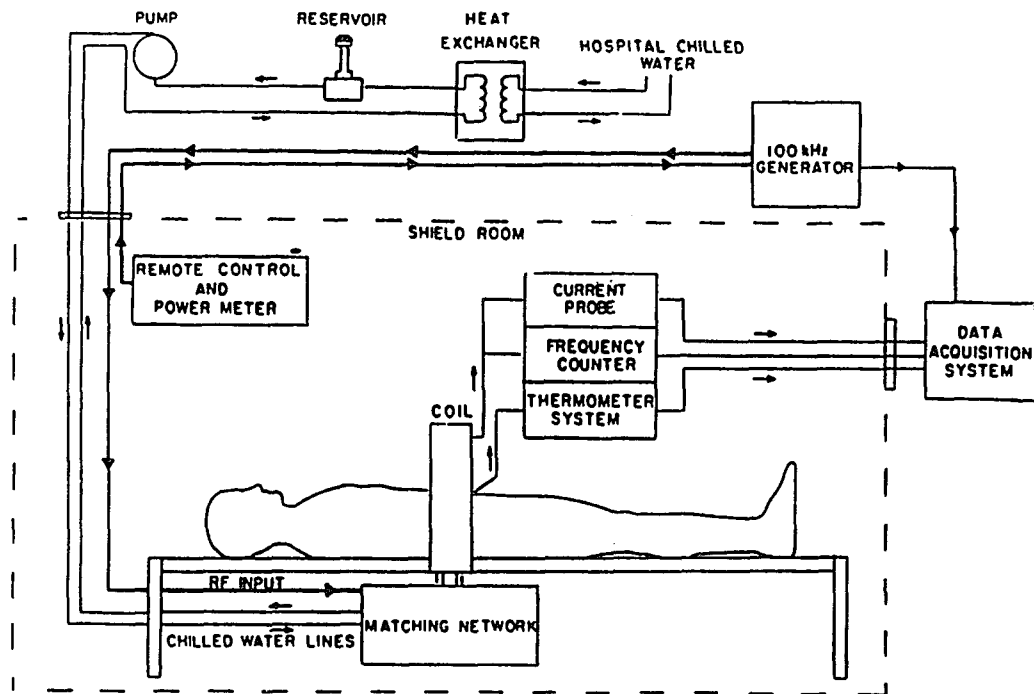
Figure 1. Magnetic induction system for heating ferromagnetic implants.

Magnetic Induction System
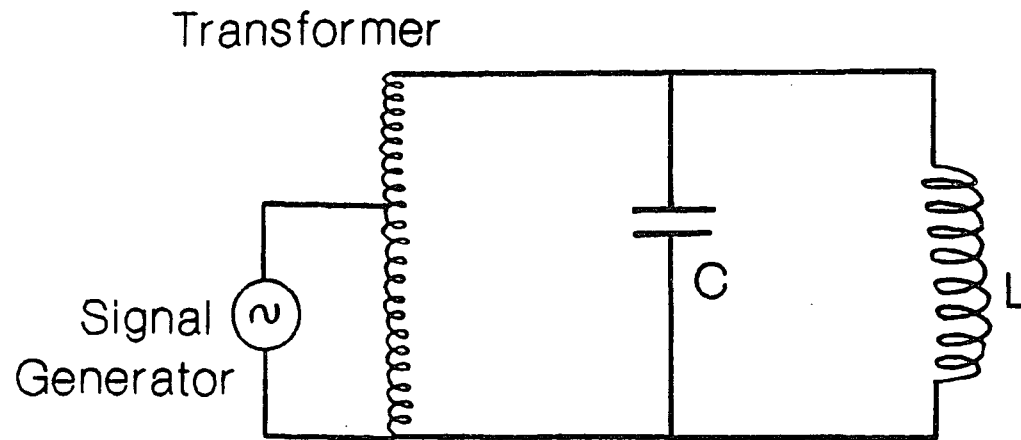
Figure 2. Equivalent circuit for the magnetic induction system.

network and coils due to the high electric currents used in the system.

6. A data acquisition system that monitors in real time both the implant temperature using thermocouples, and the power supplied by the generator.

2. Coils

The patient is placed on the treatment table and moved to the proper position within the magnetic induction coil. The coil is powered by an 8000 Watt ENI Radio Frequency (RF) generator via a matching network located under the table. The power generator is located outside the shielded room and the control area in order to avoid excessive noise in patient and technical control areas. Excessive heating in these rooms is also eliminated. A remote control panel located in the adjacent control room where the frequency and power output of the generator are controlled.

As stated above, there are three magnetic induction coils used in this system. Referring to Figure 3,

1. The C-coil: A concentric coil (60 cm aperture and 16 cm long). It encircles the patient and is used when the implants are placed parallel to the body axis. The coil constructed from copper tubing is placed in a fiberglass housing.

C-Coil
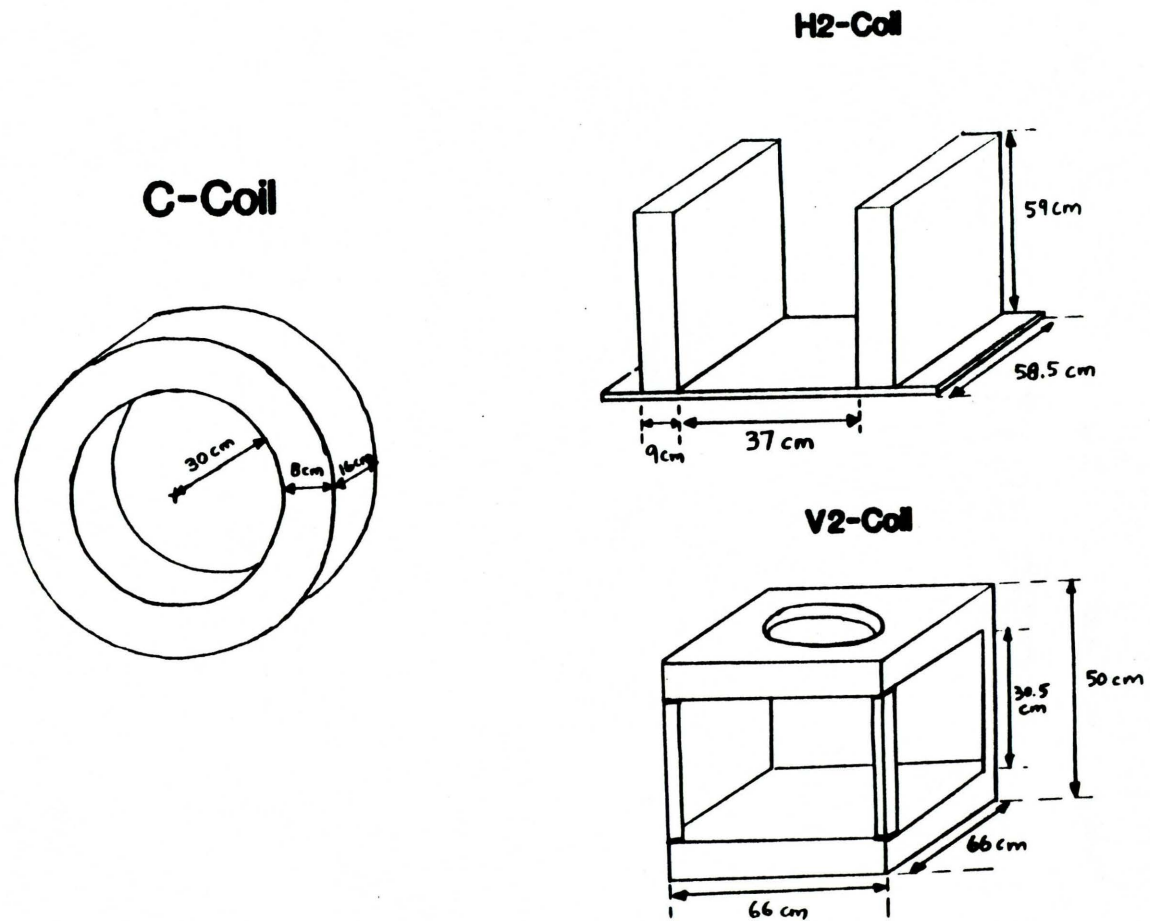
H2-Coil

V2-Coil

Figure 3. Magnetic induction coils. The C coil provides axial polarized field while the H2 and V2 coils provide horizontal and vertical polarization respectively.

2. H2-Coil: A pair of coaxially aligned coils, are mounted in an opaque plexiglass box with the top ends open for a patient to pass through. The coils are located to the sides of a patient laying flat. At least 1 cm of dielectric prevents the patient from direct contact with the coils. The magnetic field is polarized in the horizontal plane, perpendicular to the body axis. This coil is used to align the magnetic field parallel to an implant array when it is constrainted to this orientation by clinical considerations. Primarily this arises when treating certain brain tumors.

3. V2-Coil: A pair of coaxially aligned coils similar to the H2-Coil except that the coils are above and below the patient and the magnetic field is polarized in the vertical direction. The coil is boxed in a transparent plexiglass box open on three lateral sides and with a circular opening on the top side.

The C-coil was constructed first and the matching network was built to match the impedance of the C-coil to the generator. The other two coils were built to share the same matching network and have their matching frequency around 100 kHz. The important parameters here are:

1. The inductance of the coils had to be close to that of the C-coil,

2. The coils must have low resistance,

3. The field level in their centers must be high enough to

heat the implant, and

4. The field levels outside of the implant must be below hazardous amount.

Table 1 provides a summary of the electrical characteristics of the final product.

A measure of the magnetic field strength in the center of each coil is required to assure the efficiency of the coils in providing power to heat the ferromagnetic seeds. The C-coil geometry could be approximated by a two turn loop. A measurement of the current flowing through the C-coil could then provide a value for the magnetic field strength in its center and along its axis. The same could not be said for the other two coils since a derivation of the field in their centers as a function of current flowing through them is very complex. A magnetic field probe that could measure high fields at around 100 kHz is needed to map the fields in all space for any coil that is to be used with the system.

COIL	L	Z (Ohm)		MATCHING FREQUENCY
C	3.40 µH	2.17	89.89 deg	88 kHz
H2	4.40 µH	2.81	89.59 deg	80 kHz
V2	4.03 µH	2.53	89.44 deg	82 kHz

Table 1. Electrical characteristics of the 3 coils used for magnetic induction. (L and Z are measured at 100 kHz).

CHAPTER 3

OPTICALLY COUPLED MAGNETIC FIELD PROBE

An optically coupled magnetic field probe discussed here is an apparatus for measuring the field strength of the magnetic induction coils and surveying the magnetic field strength throughout the treatment room.

1. Fundamentals of R.F. Magnetic Field Measurement

The direct measurement of R.F. magnetic field with a sensing loop or coil is based on Faraday's law of induction. In some systems[4,5], the voltage induced in the pick up coil is measured directly and calibrated against the field present in the sensor as in Figure 4. Such measurement systems have the following problems:

1. The unpredictable effect of strong magnetic fields on the measuring instrument (the voltmeter in the case of Figure 4),

2. The presence of induced voltages on the connecting leads from the sensor to the instrumentation that produces artifacts in the field measurement,

3. Currents along these leads can actually perturb the field that we are trying to measure.

These problems could be overcome by using an optical link

Direct field measurement
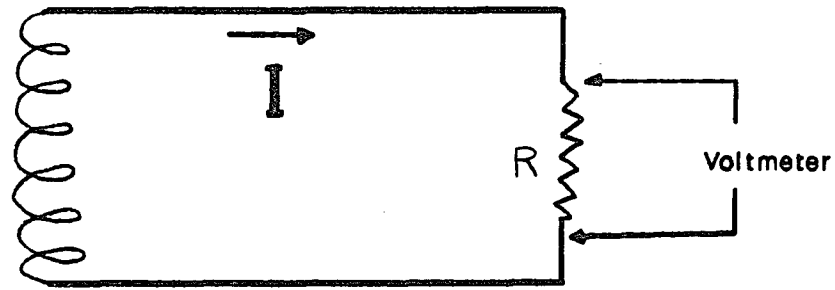
Figure 4. Non optical magnetic field measuring sensors.

between the sensor and the signal processing instrumentation and locating the instrumentation outside the shielded room.

A field probe is built after a model provided by Eugene Gross[3] working at 13.56 MHz. The new probe is optimized for 100 kHz frequency, uses a different approach for temperature compensation and while using the same optical detector circuitry, an R.F. filter is added inside the detector box reducing the R.F. interference to negligible levels. The probe employs a passive sensor to monitor strong R.F. magnetic fields: the magnetic field is picked up by a small coil which generated a voltage across its terminals. This induced voltage drives an LED which emits an optical signal proportional to the magnetic field under test.

2. Probe Sensor Design

A good understanding of LED devices is necessary in order to provide an accurate probe. The forward current rating for the LED used here is 100 mA as published by the manufacturer[6]. However, the reverse bias operation is limited to 25 mA. An excess of this value could result in catastrophic failure of the device. Since we are using an AC signal, a protection diode mounted with reverse polarity across the LED is necessary. This limits the reverse bias of the LED to about 0.7 volts, which is well below the reverse

breakdown (valued at about 10 volts).

A resistor in series with the LED is used to limit the current flowing through it and thus preventing it from being damaged. The value of this resistor is calculated from the expected voltage across the LED and the current limit of 10 mA through the LED. The voltage across the LED is determined from Faraday's law by the equation

$$V = N \mu w \pi r^2 H$$

where

N = number of turns in the pick up coil,

μ = permeability of free space,

w = angular frequency of the signal,

r = radius of the pick up coil, and

H = the magnetic field strength in the pick up coil.

For N=73 turns, w=$2\pi 100 \times 10^3$ and r=0.012 m, Table 2 gives the voltages across the LED for given values of the magnetic field strength H. As can be seen from this table, for an H field of 3000 A/m, the voltage across the LED becomes 78.21 volts. In order to limit the current through the LED to 10 mA, the value of the series resistor should be

$$Rd = (78.21 \text{ V})/(10 \text{ mA}) = 7.821 \text{ KOhm}$$

Another characteristic inherent in an LED device is its sensitivity to temperature. Proper temperature compensation is therefore required for an accurate device.

H-FIELD (A/m)	VOLTAGE ACROSS LED (V)
200	5.21
400	10.42
600	15.62
800	20.86
1000	26.07
1200	31.28
1400	36.50
1600	41.71
1800	46.63
2000	52.14
2200	57.35
2400	62.57
2600	67.80
2800	73.00
3000	78.21

Table 2. Calculated voltage across the LED for given field strength in the pick up coil of the optically coupled magnetic field probe. The frequency here is 100 kHz.

3. Temperature Compensation

Temperature sensitivity of the LED creates unreliable or unstable measurement of the magnetic field strength. Due to the complex nature of this sensitivity (caused by variation in injection efficiency, band gap dependence on the junction level and other mechanisms), an empirical determination of the thermal behavior of the LED is performed and a suitable compensation technique is presented.

As the LED's intensity provides the measurement signal, temperature drifts during the measurement of a stable R.F. magnetic field gives an indication of the LED's sensitivity to temperature. The circuit comprising of the pick up coil, the LED, the protection diode and a 7.821 KOhm resistor in series are placed in a copper cylinder thermally isolated (Figure 5). A nichrome wire is wound around the cylinder which heats up when subjected to a current through it. This current is precisely controlled using a feedback thermistor placed inside the copper cylinder giving a stable temperature throughout. Providing an R.F. magnetic field inside the thermal system is nearly impossible because of the shielding effect of the copper. An alternative method of exciting the LED is sought. A known AC voltage is injected in the probe system (at point 1 and 2 in Figure 8) to mimic

Temperature sensitivity setup
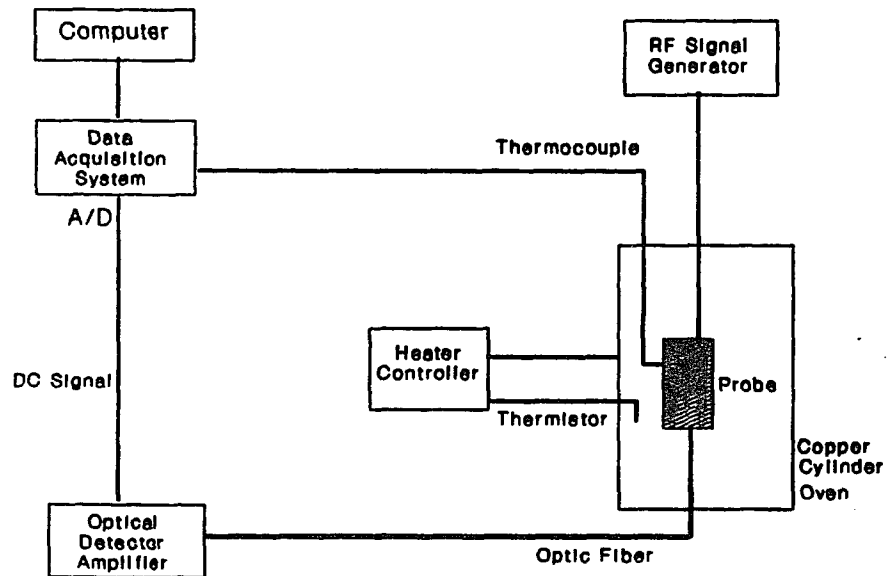
Figure 5. Experimental setup for determining the temperature sensitivity of the LED.

Temperature Sensitivity
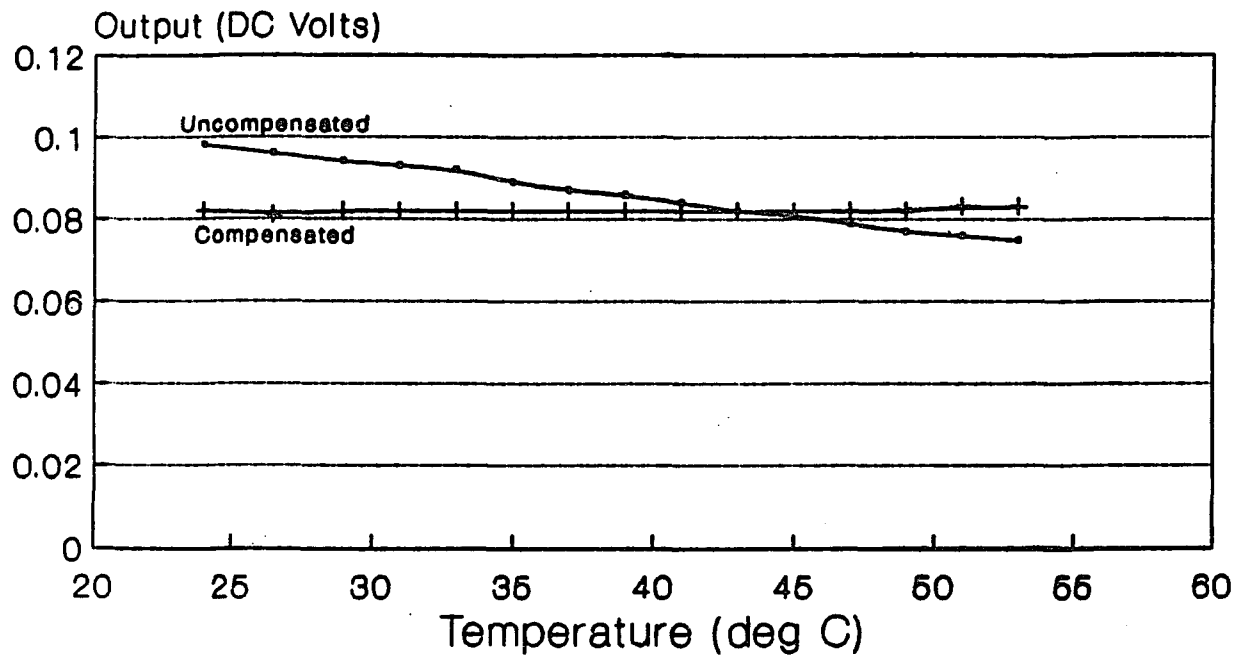
Figure 6. Graph of the temperature sensitivity of the LED showing
the output of the photo detector/amplifier versus the temperature
of the copper cylinder oven.

Current Distribution

Current

Distance
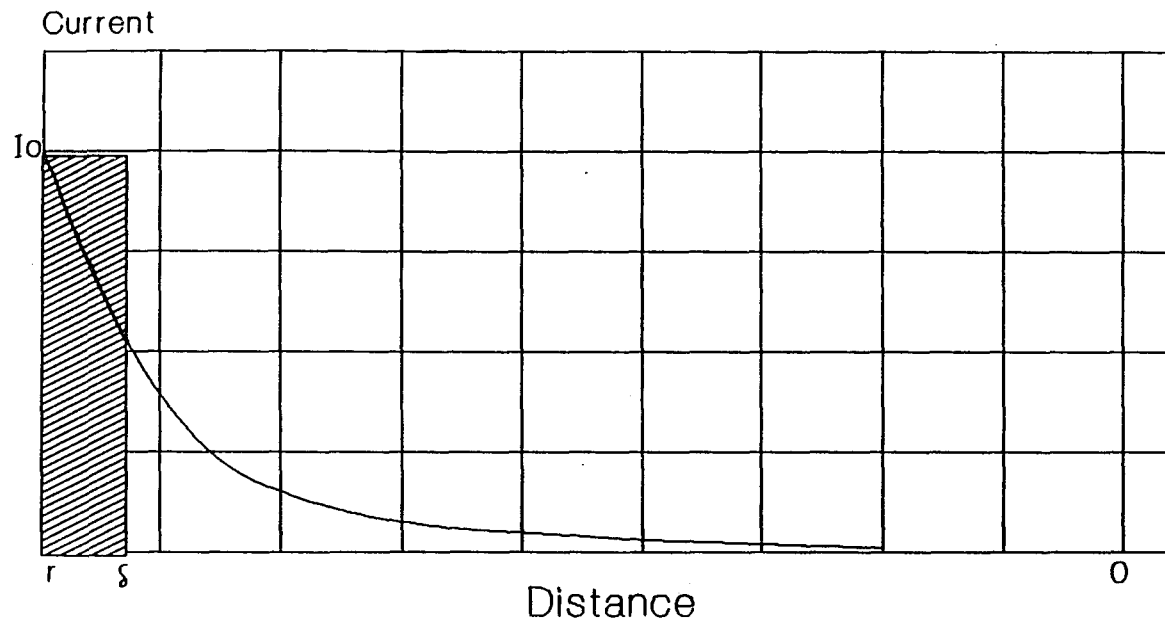
Figure 7. Current distribution in a cross-section of a seed.

Final Circuit
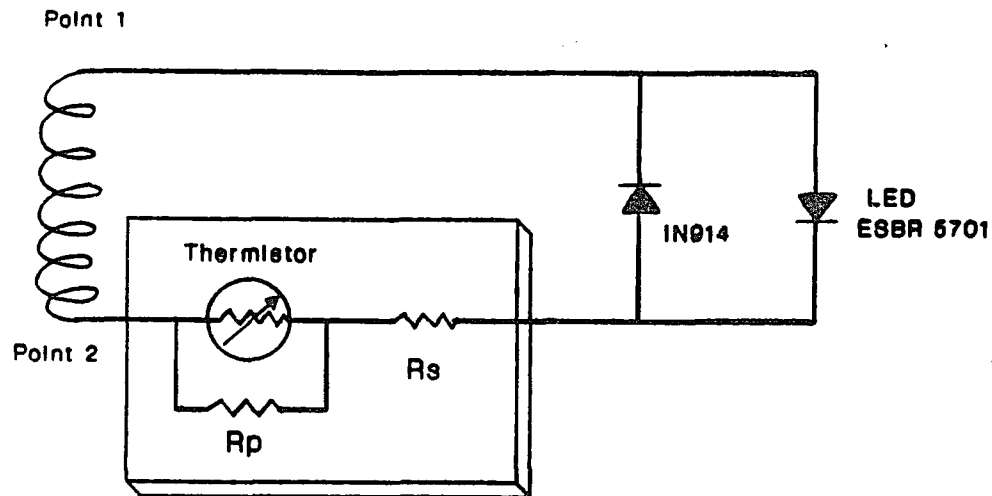
Figure 8. Final Schematic diagram of the optically coupled magnetic field probe.

the induced voltage in the coil while the latter is disconnected. With the aid of an HP 9836 data acquisition system, temperature sensitivities were determined. Figure 6 shows a graph of the LED output as a function of temperature when a constant AC voltage is used as input. Ideally, for a zero temperature coefficient, the curve should be a horizontal straight line. This is the goal sought by temperature compensation.

Temperature compensation of semiconductor junctions can be achieved by using the linearizing thermistor network suggested by Jaffe[7]. A complete description of the technique is presented in Appendix A. The results yield excellent temperature independence as depicted in Figure 6.

The final circuit of the magnetic field probe is given in Figure 8.

4. Probe Construction

The optically coupled magnetic field probe uses a 73 turn detection coil because the use of a single turn loop of small diameter (1 cm) does not provide enough voltage to drive the LED. The entire field sensor is packaged in an Amphenol optical bulkhead receptacle. The LED is drilled from the leads side with a number 60 drill bit very close to the junction. The thermistor is embedded in the hole and covered with epoxy. The LED head is filed flush with the

surface, polished, and fitted snugly in the bulkhead receptacle. The pick up coil is wound on a Teflon cylinder and placed over the receptacle. Electrical connection are made, and the entire probe is filled with opaque epoxy.

5. Optical Link and Photo-amplifier

The optical link is built per Amphenol instructions[9] by using a Galite 2000P bundled optic fiber polished and mounted on the receptacle.

The detector circuit was one designed and built by Eugene Gross[3]. It comprises a photo-detector, two chopper stabilized operational amplifier stages and an Analog to Digital converter (A/D) with display drivers (Figure 9). The second operational amplifier serves as a buffer between the first current amplifier and the A/D. It was replaced by an LM 740 operational amplifier after the initial one failed. The circuit is powered through an R.F. line filter so it can be used inside the shielded room.

6. Calibration of the Field Probe

The calibration of the optically coupled magnetic field probe is performed by comparing the reading output of the detector against known fields.

An R.F. magnetic field is created by passing a current through a solenoid. The geometry of the solenoid and

Detector circuit
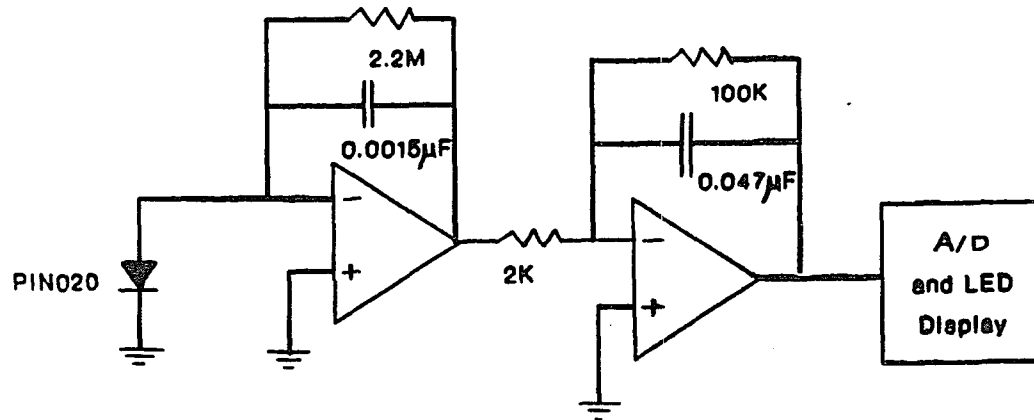
Figure 9. Details of the assembly of the photo detector /amplifier circuit showing also the display unit.

a measurement of the current enables the calculation of the strength of the magnetic field.

Referring to Figure 10, the computerized data acquisition system (DAS) controls a signal generator model HP 8656B that feeds a sine wave at 100 kHz to a power amplifier model ENI 1140LA. The output of the amplifier supplies the current to a tuned series RLC circuit. By feeding the voltage across the resistor R to the DAS, the magnitude of the current is determined. Because we have a tuned series circuit, this is also the current in the solenoid. The DC output of the probe detector is concurrently supplied to the DAS. A capacitor with a 38.2 nF capacitance at 100 kHz and a voltage handling of 1,500 volts was on hand, the value of the needed inductance of the coil is then calculated from

$$w = 1/(LC)^{1/2}$$

where w is the angular frequency of the tuned circuit. Then, L = 66.2 μH.

A solenoid is constructed to have this value of inductance. It has a length of 30 cm, a diameter of 5.5 cm and 86 turns of 14 AWG wire as shown in figure 11. The dimensions of the solenoid are therefore adequate to fit the optical probe in its center.

The termination resistance R is actually two Dale power resistors in parallel with a value of 98 ohms each at

Field Calibration Setup
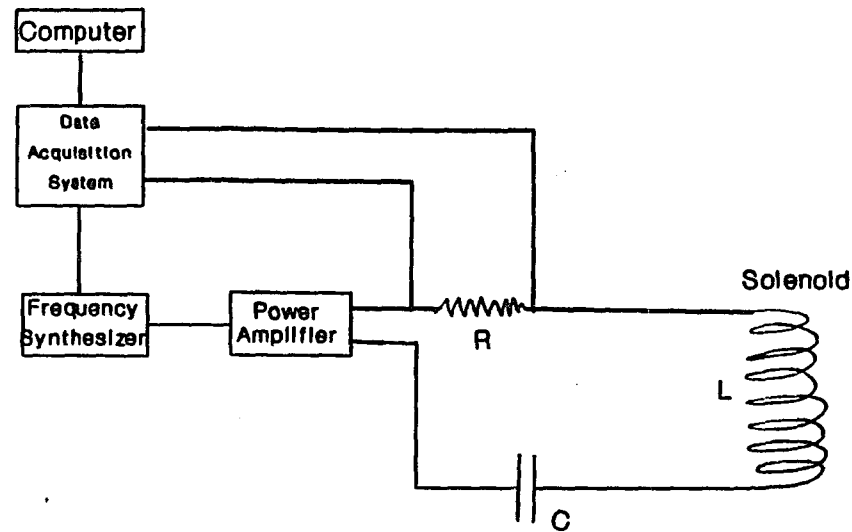
Figure 10. Experimental setup for calibration of the optically coupled magnetic field probe. The probe is positioned in the middle of the solenoid.

Solenoid Construction

5.5 cm

30 cm

Number of Turns = 86
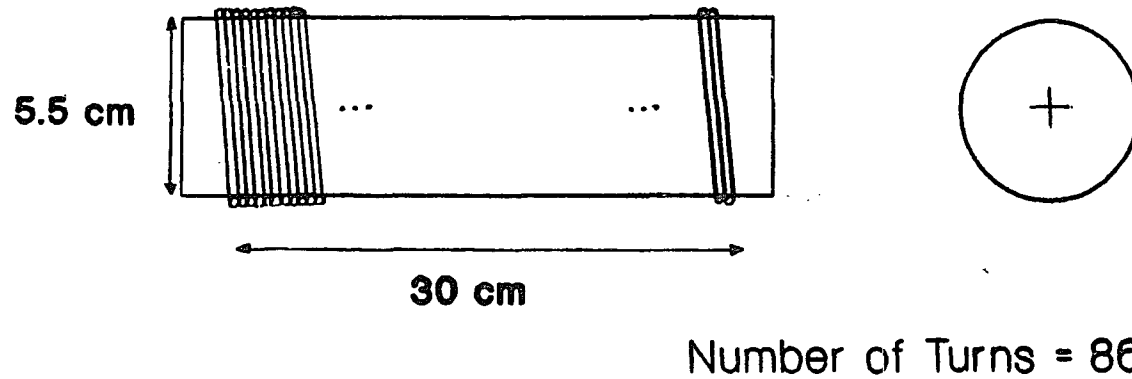
Figure 11. Details of the construction of the solenoid used for calibration of the field probe.

Optical Probe Calibration
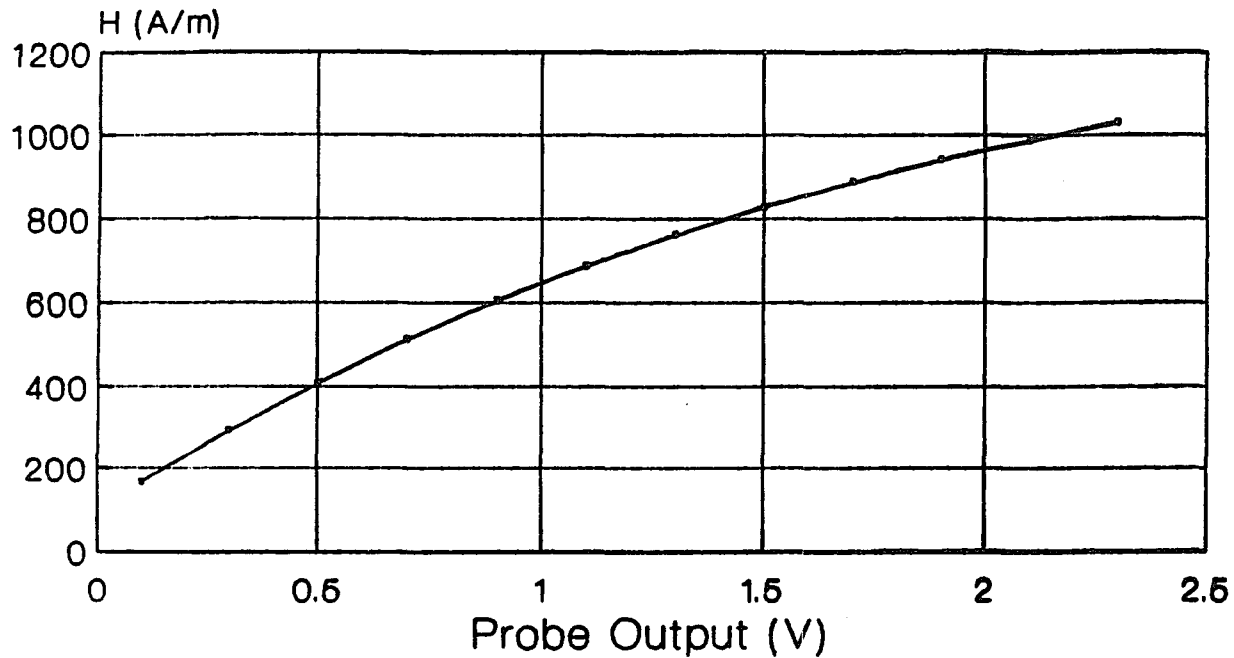
Figure 12. Results of the calibration of the H field probe at 100 kHz. H(A/m) = 1387.8 - 1293.5 EXP[-0.55858 Vopt]

Optical Probe Calibration
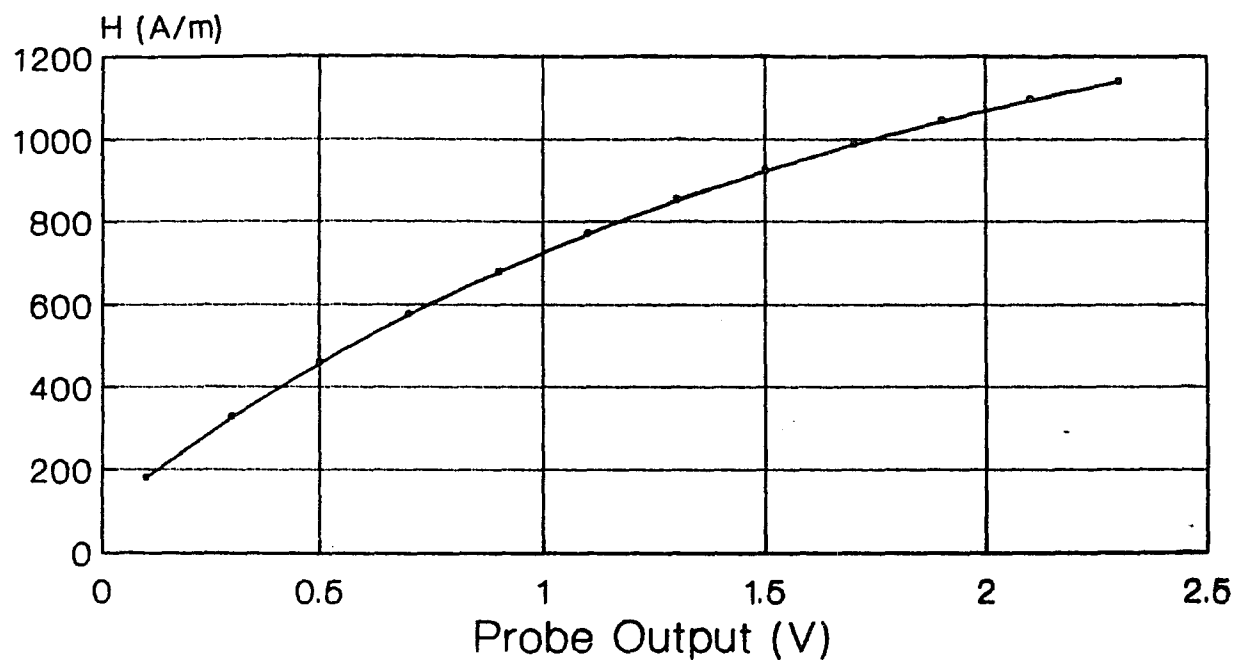
Figure 13. Results of the calibration of the H field probe at 90 kHz. $H(A/m) = 1488.6 - 1390 \, EXP[-0.60007 \, Vopt]$

Optical Probe Calibration
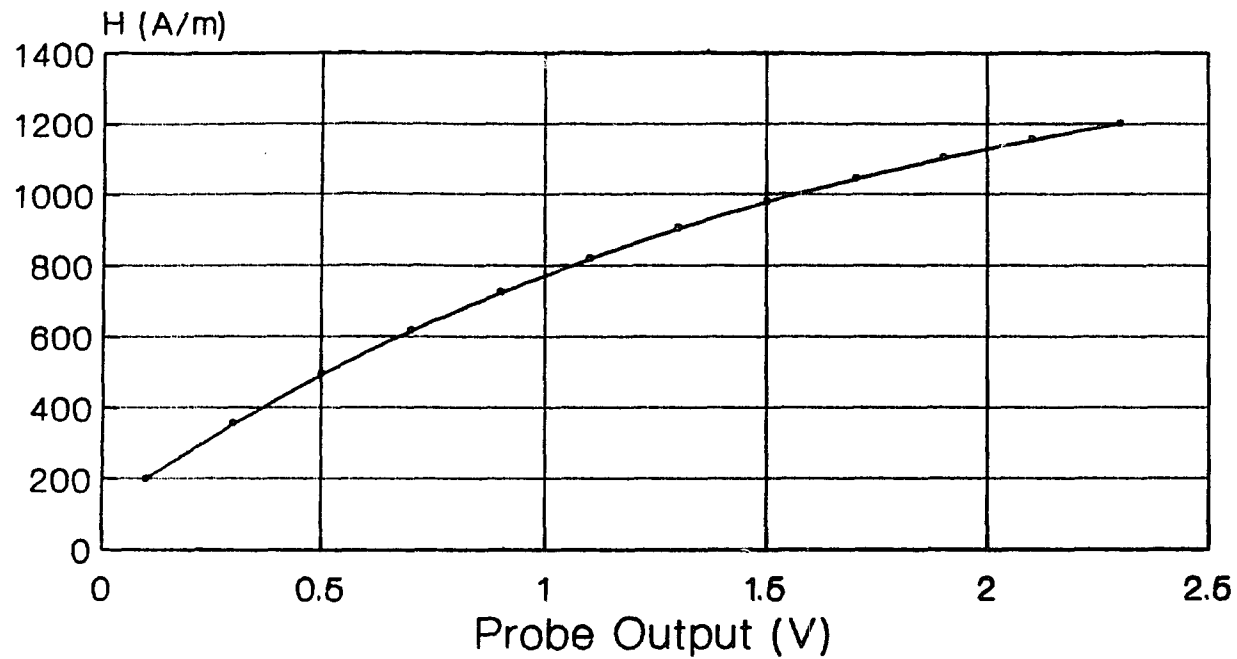
Figure 14. Results of the calibration of the H field probe at 85 kHz. H(A/m) = 1548.9 - 1436 EXP[-0.061518 Vopt]

Optical Probe Calibration
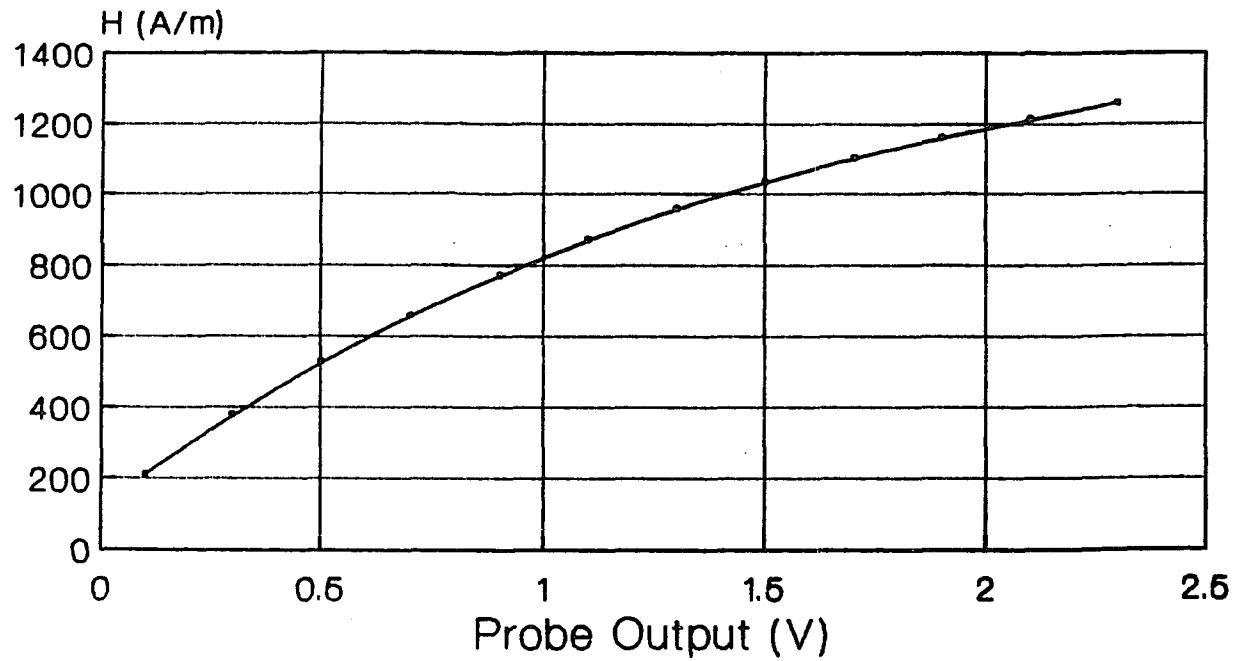
Figure 15. Results of the calibration of the H field probe at 80 kHz. H(A/m) = 1578 - 1462.5 EXP[-0.65983 Vopt]

100 kHz, giving the complete circuit a total impedance of 50 Ohms resistive around 100 kHz.

From Biot-Savart law applied to a finite solenoid with n turns per unit length, the magnetic field strength in the middle of the solenoid is approximated by

$$H = n.I$$

where I is the current flowing in the windings.

The calibration procedure is the following: first, the optical field probe is inserted in the middle of the solenoid. Then the signal generator is made to increase in steps its current output on the command of the DAS. The voltage across the resistor R is measured by the DAS and converted to a value of the magnetic field strength H. At the same time, the output of the probe detector Vopt is read by the DAS. The results of such a calibration are plotted in Figure 12. The data points are subsequently curve-fitted using an exponential model of the form

$$H \ (A/m) = P(1) + P(2).e^{[Vopt.P(3)]}$$

where

H is the strength of the magnetic field,

P(1), P(2), P(3) are the calculated curve fit parameters,

Vopt is the output voltage of the probe detector.

The calibration is repeated for input frequencies of 90, 85 and 80 kHz and is plotted in Figures 13, 14 and 15 respectively.

7. System Characteristics

Some characteristics of the optically coupled magnetic field probe are discussed in this section. These are, sensitivity and dynamic range of the probe, bandwidth and susceptibility to electrical field.

Sensitivity and dynamic range are not separate quantities for the optical field probe system. Altering the sensitivity of the sensor will affect its useful range. The two are affected by the value of the series resistance (the temperature compensation network) and the sensing coil of the probe. If the series resistance is increased, the sensitivity is decreased while the dynamic range is increased. An increase in the aperture of the pick up coil or its number of turns increases the sensitivity but decreases the dynamic range. In these adjustment note that there is a threshold voltage for the LED to be considered. This threshold is 1.7 volts for the Stanley ESBR5701 LED used[6]. In addition to that, the current through the sensor should remain under 10 mA to avoid self heating of the temperature compensation thermistor network.

The probe was found to be dependent on the frequency of the field measured. The calibration of the probe presented above at 10 kHz intervals between 80 and 100 kHz is adequate to cover the frequency range used for the magnetic induction system. The relation of field strength

against the output of the probe detector is not an obvious one. The use of the probe at a different frequency should be preceded by a calibration at the frequency to be measured. Note that the probe is optimized for frequencies around 100 kHz.

The pick up coil is wound using one layer of wire in a static fashion. This makes the probe sensitive to electric fields in addition to magnetic fields. The value of this sensitivity is not determined but assumed to be small because of the short length of the coil and its low resistance. Future probes should be wound astatically using two layers of wire to make them indifferent to levels of electric field.

CHAPTER 4

ELECTRIC FIELD MEASURING INSTRUMENT

This chapter is devoted to the description of the electric field probe used for mapping the electric field generated by the magnetic induction system in the shielded room. The measuring instrument is a commercial unit manufactured by Holaday Industries Inc. The model number is HI-3600 Radiation Survey Meter on loan to the Department of Radiation Oncology by Reed Holaday.

1. Principle of Operation

The HI-3600 is a single polarization field strength meter. It directly displays the root-mean-square (RMS) value of the electric field on a liquid crystal display (LCD) screen and also on a remote LCD unit linked to the main unit via digital fiber optic communication. Electric fields are measured using a displacement current sensor. The displacement current sensor operates on the principle that when two electrically connected parallel conductive flat plate electrodes are immersed in an electric field, they will exhibit a displacement current flowing between the two plates and proportional to the electric field. This can be visualized by remembering that no electric field exist

between two such plates when they are connected together, because they are at the same potential. But when immersed in an electric field, the external field causes a redistribution of electric charges between the two electrodes which is in reality just a flow of current. A measure of this current provides a measure of the external electric field.

2. Characteristics

The Electric field probe has two 20 cm circular plate sensors. Its is able to measure fields in the range 0.05 to 1999 volts/meter. The frequency response of the probe is from 10 kHz to 100 kHz at +/- 0.5 dB and 2 kHz to 300 kHz at +/- 2 dB.

CHAPTER 5

FIELD MAPPING

The electric field probe on loan and the newly built magnetic field probe are used for mapping the fields in the shielded room with the three different magnetic induction coils. In this chapter, the results of the mappings are presented.

1. Magnetic field strength results

Measurements of the magnetic field strength in the center of the magnetic induction coils is needed to determine their efficiency. The results of these measurements are presented in Figures 16, 17, and 18 for the C, H2 and V2 coils respectively. The figures show the plots of the square of the magnetic field strength against the forward power read on the remote control box of the generator. The meter is an analog display of the forward and reflected powers in watts. The plot is linear as expected and a linear regression is carried out to curve fit the data points. The results of the curve fitting routine are the following

For the C coil, $H^2 = 672.P + 79331$

For the H2 coil, $H^2 = 442.P + 58283$

C-Coil measurement
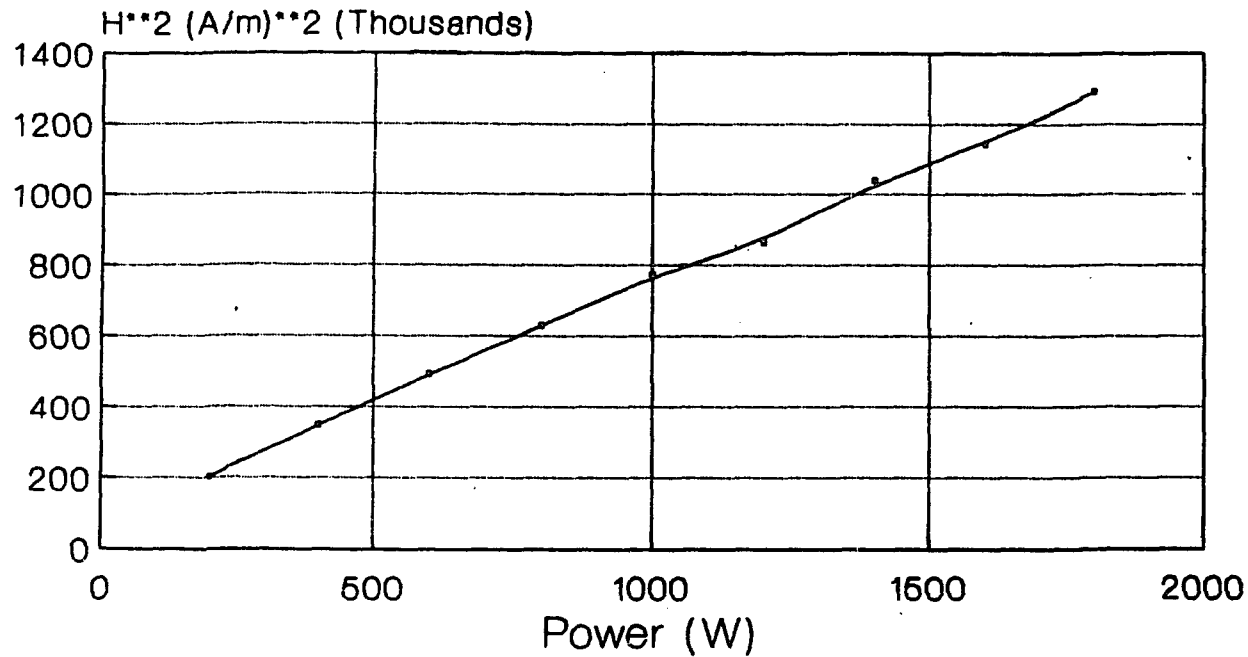
Figure 16. Graph of the performance of the C coil showing the square of the magnetic field at the center of the coil versus the power applied.

H2-Coil measurement
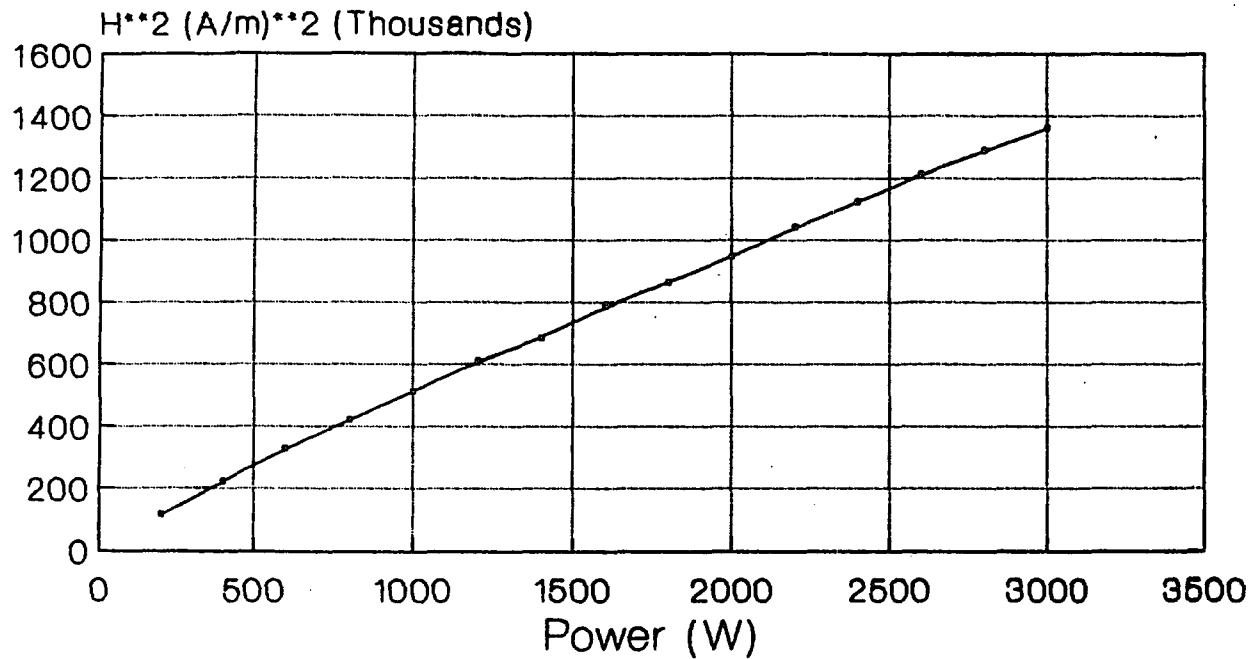
Figure 17. Graph of the performance of the H2 coil showing the square of the magnetic field at the center of the coil versus the power applied.

V2-Coil measurement
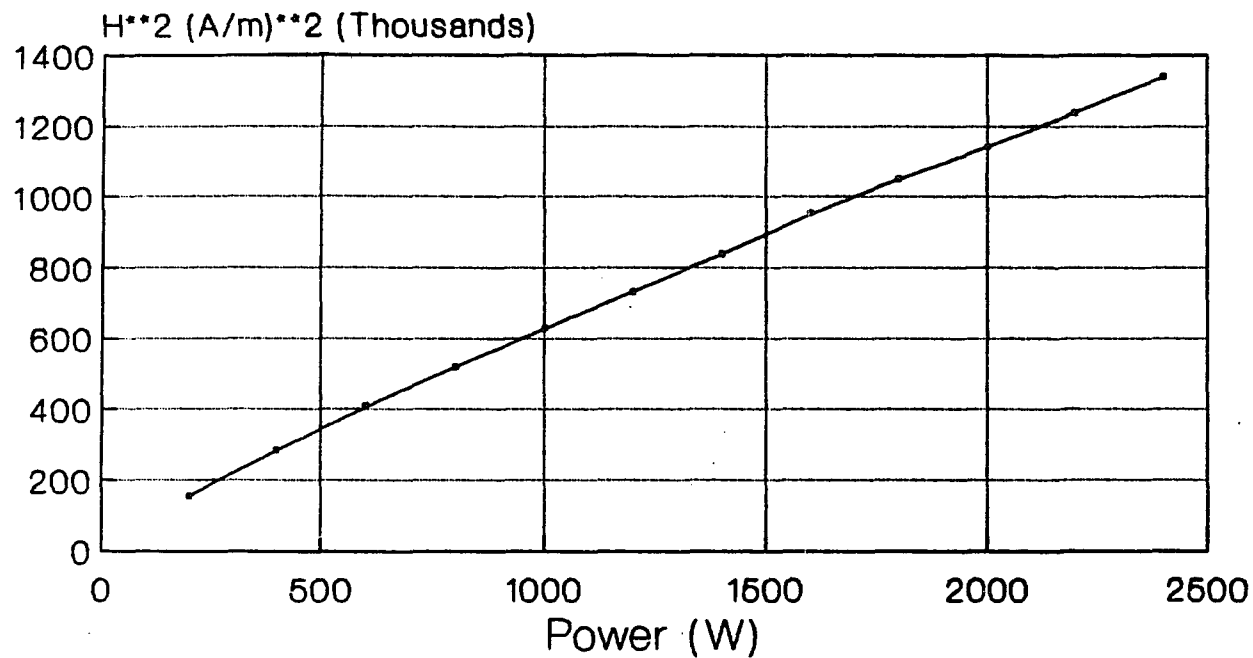
Figure 18. Graph of the performance of the V2 coil showing the square of the magnetic field at the center of the coil versus the power applied.

For the V2 coil, $H^2 = 533.P + 79060$

where H^2 is in $(A/m)^2$ and P in watts.

Stauffer[12] found an experimental lower limit of the magnetic field strength at about 800 A/m for a system similar to the one used here but running at 1.9 MHz. He also calculated an expression of the power absorbed by the implant given by

$$Pi = [\pi \, a(2)^{-1/2}] (wu/\sigma)^{1/2} \; Ho^2$$

where a is the radius of the implant, w the angular frequency, Ho the applied magnetic field strength, μ and σ are the permeability and the conductivity of the implant respectively.

In order to keep Pi constant at the desired frequency of 100 kHz, the new value of Ho is computed from

$$Pi_a/Pi_b = (a/b)^{1/2} \; (Ho_a/Ho_b)^2$$

where a is for 1.9 MHz and b for the 100 kHz frequency.

For equal power, this gives

$$1 = (1.9/0.1)^{1/2} \; [(800 \; A/m)/(Ho_b)]^2$$

=> $Ho_b = 1670$ A/m

From the equation of the square of the magnetic field strength against the power observed on the generator controller, we can calculate the power required from the generator for heating the implant using the different coils:

For the C coil this value is P = 4000 watts,

For the H2 coil, P = 6100 watts,

For the V2 coil, P = 5100 watts.

Note that the generator is able to supply up to 8000 watts of power which is therefore more than enough for successful heating using any of the coils.

2. Comparison Between Measured and Theoretical Values

The following is a comparison between measured and theoretical values for the square of the magnetic field strength for the C coil along an axis going through the center of the coil and parallel to the treatment table. The measured values are those detected by the optically coupled field probe and the theoretical values are calculated from the following analysis:

Assuming that the C coil is a two turn circular loop, and referring to Figure 19,

The plane of the loop lies in the xy plane with center at the origin and loop axis coincident with the z axis. The contribution of a small segment dl to the magnetic field on the axis is given by[13]

$$dH = \frac{1}{4\pi} \cdot \frac{I \times R}{R^2} \cdot dl = \frac{I \cdot dl}{4 \pi R^2}$$

The last term is obtained because R is orthogonal to any I.dl in this geometry. The dH field of current element I.dl is at right angles to R, but when we consider the

C-Coil Approximation
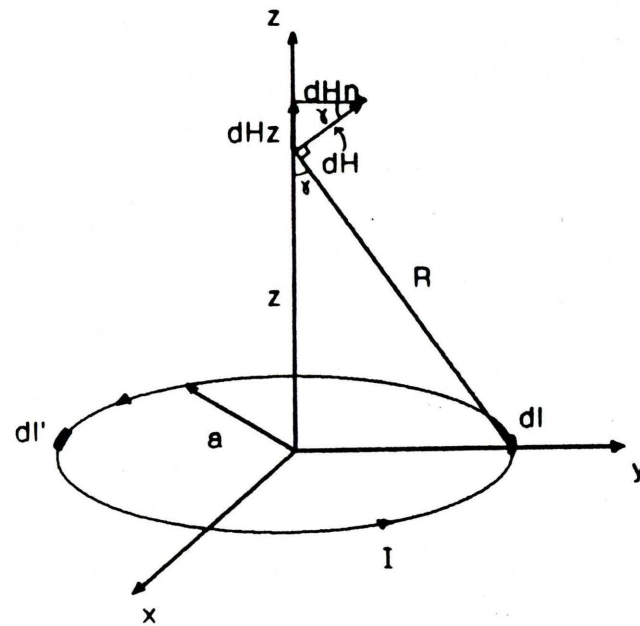
Figure 19. A current loop of radius a produces an H field along the loop axis with a z component only.

contribution dH' from a diametrically opposite element dl·',
we see that the dHn components which are perpendicular to
the axis cancel. As a matter of fact, since this
cancellation occurs for all diametrically opposite pairs of
dl elements around the loop, only the component dHz = dH.sinγ
parallel to the loop axis remains. The total field is given
by summing all dHz,

$$Hz = \int dHz = \frac{I.\sin\gamma}{4.\ R^2} \oint dl$$

$$= \frac{I.a^2}{2.(z^2 + a^2)^{3/2}} \qquad \text{Equation 1}$$

For a two turn loop, this expression becomes

$$Hz = \frac{I.a^2}{(z^2 + a^2)^{3/2}}$$

For a = 30 cm and a field strength measured using
the optically coupled field probe at z = 0 to be 701.16 A/m
with 600 W of input power, we can retrieve I from the above
equation, I = 210.35 A. Knowing the current flowing through
the coil at 600 W, a fit of the calculated square of the
magnetic field strength along the axial direction is
superimposed on the measured values in Figure 20.

Position (cm)	H^2 Measured Values $(A/m)^2$	H^2 Calculated Values $(A/m)^2$
-55	10904.88	5927.22
-50	16883.64	9118.71
-45	26814.54	14321.66
-40	44353.66	22937.71
-35	73172.83	37350.23
-30	116587.52	61454.34
-25	171996.78	101055.63
-20	251256.97	163132.31
-15	337344.22	251716.95
-10	419812.00	358401.69
-5	472423.06	452840.06
0	491619.19	491619.19
5	460539.97	452840.06
10	385346.53	358401.69
15	307854.50	251716.95
20	220863.28	163132.31
25	153611.03	101055.63
30	102791.43	61454.34
35	65432.54	37350.23
40	39620.04	22937.71
45	25526.60	14321.66
50	16253.44	9118.71
55	10560.49	5927.22

Table 3. Comparison between measured and theoretical values of the square of the magnetic field strength for the C coil, along its axial position.

C-Coil Axial Mapping
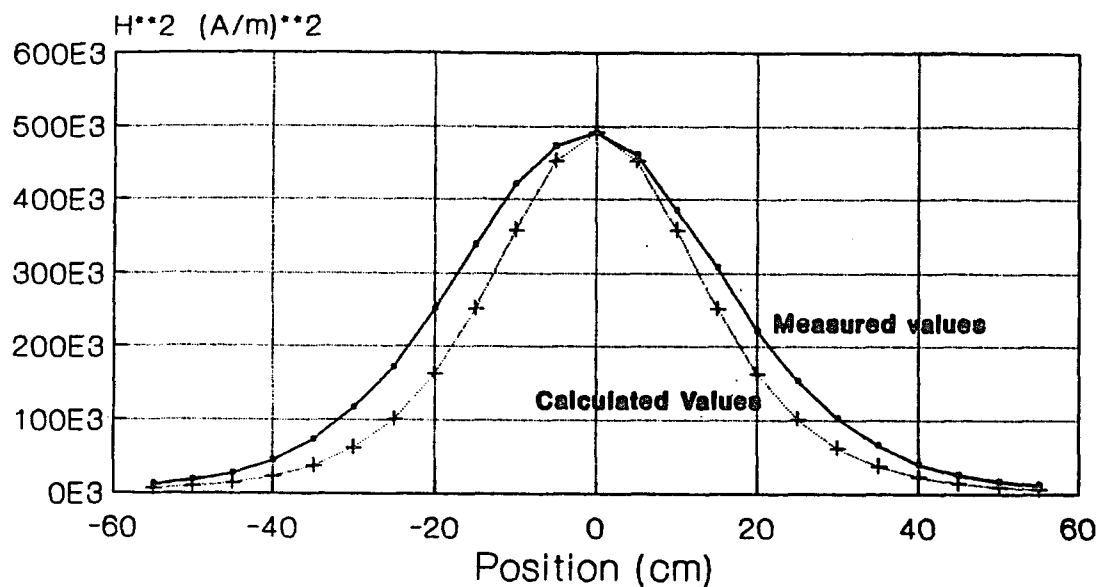
Figure 20. Comparison between measured magnetic field strength using the optically coupled probe and calculated values from the two turn loop approximation of the C coil.

The Figure shows a small difference in the field strength between the measured and calculated values. The measured values are slightly higher. This is because the mathematical derivation does not consider the appreciable thickness of the C coil (16 cm). The effect of this thickness is higher fields at close axial distances from the center of the coil. When this distance increases, the thickness effect vanishes and the above equation becomes a better approximation. This is indeed what is observed in Figure 20.

Mappings of the C coil in the axial and radial directions are shown in Figures 21 and 22. Both these mappings are carried out using the optically coupled magnetic field probe and at 600 watts of generator power. The significance of these results will become apparent in the next chapter when the field levels for personnel safety are discussed.

3. Electric Field Results

The Holaday electric field probe is used to map the fields generated by the magnetic induction system. Although these fields do not have an appreciable contribution to the ferromagnetic seed heating, their measurement is important for safety reasons discussed in the next chapter. The Holaday probe measures fields using a single polarization.

C-Coil Axial Measurement
600 W, frequency: 88KHz
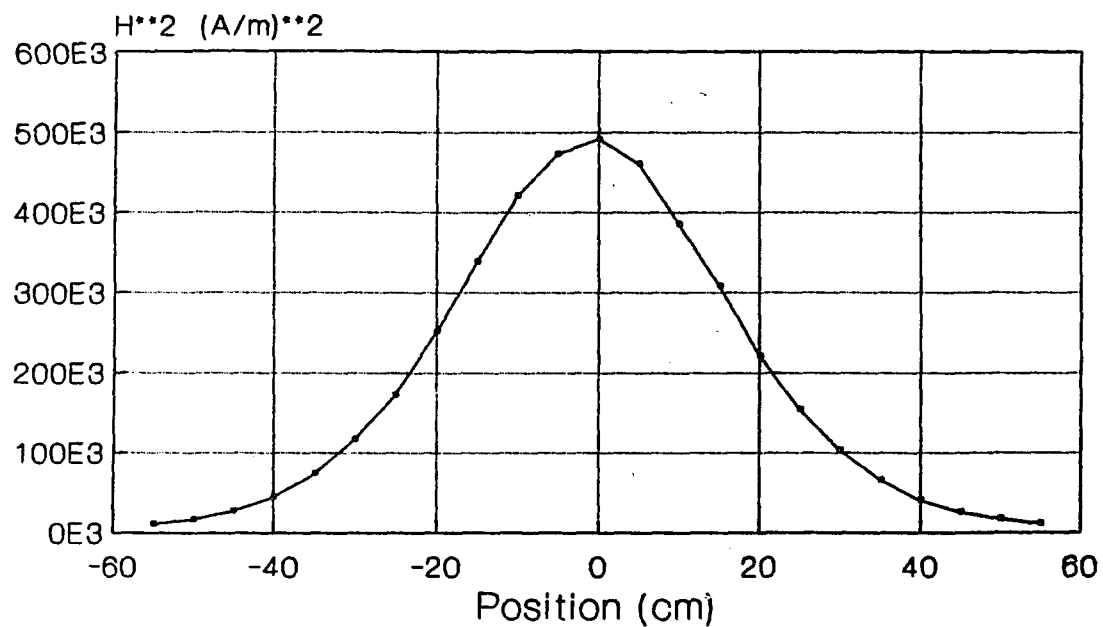
Figure 21. Magnetic field strength as a function of the axial position using the C coil at 600 W power.

C-Coil Radial Measurement
600 W, Frequency: 88 KHz

H**2 (A/m)**2 (Thousands)
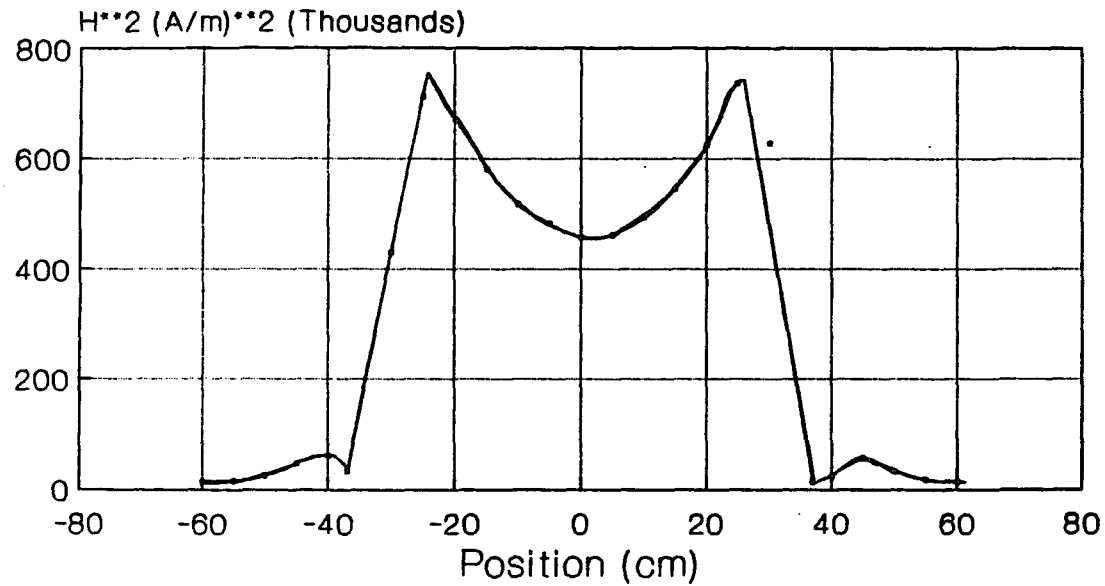
Position (cm)

Figure 22. Magnetic field strength as a function of the radial position using the C coil at 600 W power.

The characterization of the fields present in the shielded room require measurements on the three orthogonal polarization. Figure 23 shows such measurements at the center of the C coil against the forward power of the generator as read on the remote controller. Additionally, Figure 24 shows the mapping of the electric field along the axis passing through the center of the coil and parallel to the treatment table. Note that the highest contribution to the electric field is along the z polarization with its highest value 50 cm behind the magnetic induction coil this is the location of the matching network in the room. This suggests that it is the matching network or the potential between the coil and the matching network that are responsible for the highest field levels.

E-Field Plots C-Coil

E-Field (V/m)

Power (Watts)

- • X Polarization   + Y Polarization   * Z Polarization
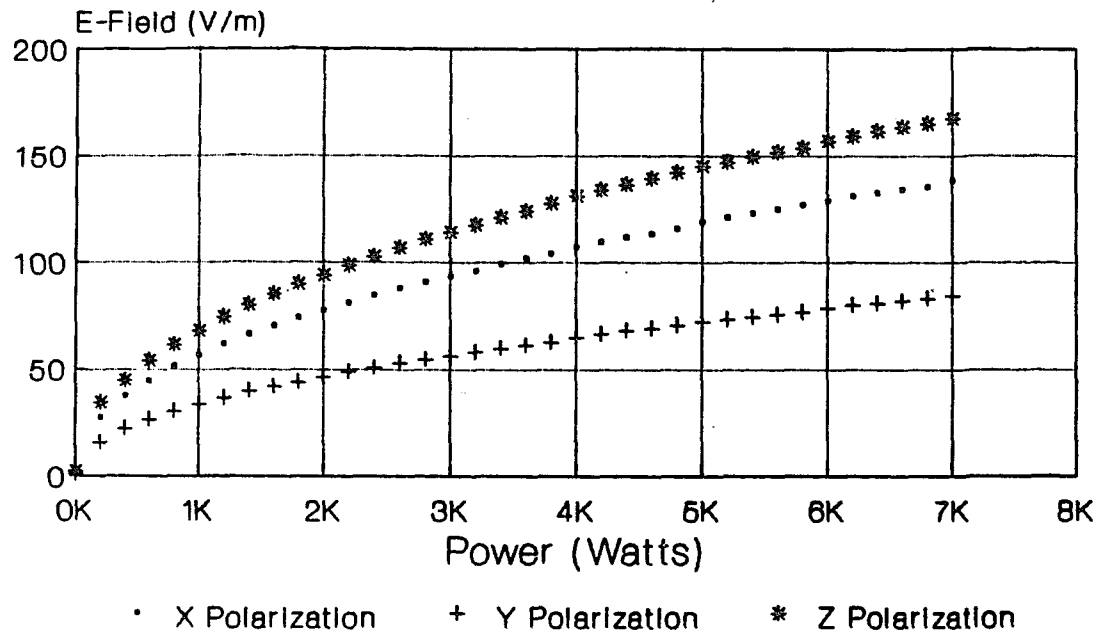
Figure 23. Electric field measurement using the Holaday probe versus power using the C coil.

E-Field Mapping
C-Coil

E-Field (V/m)
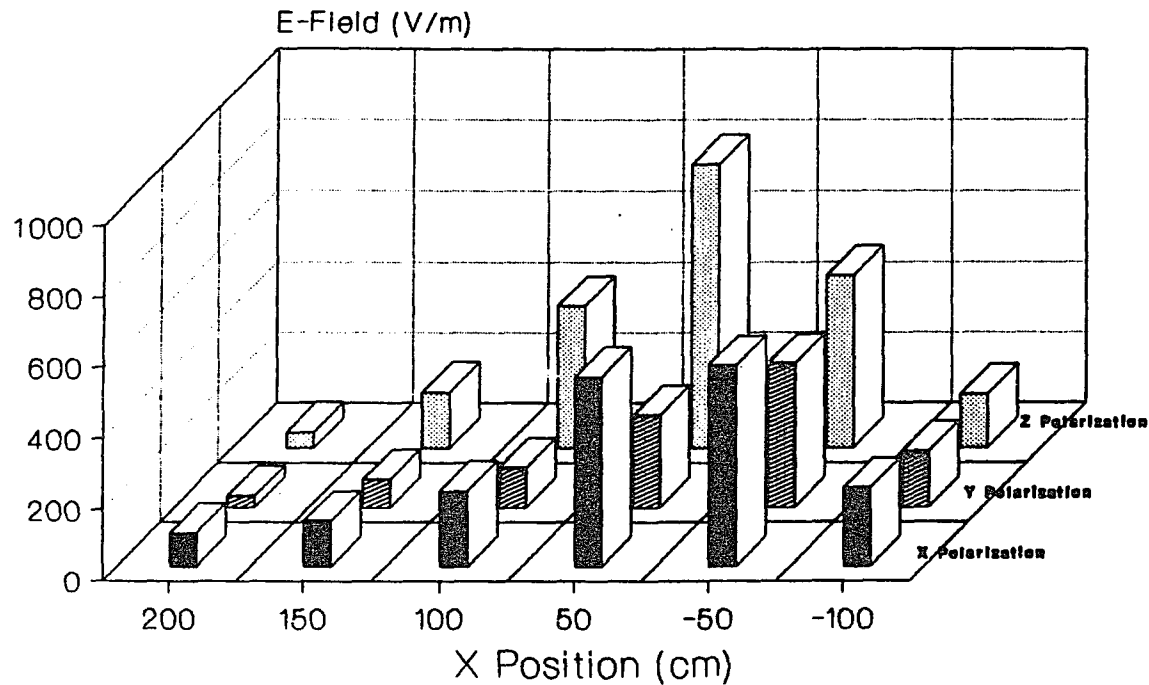
Power: 6000 Watts

Figure 24. Electric field measurement using the Holaday probe versus axial position using the C coil at 6000 W. The graph shows the electric field in the 3 polarizations.

CHAPTER 6

MAGNETIC AND ELECTRIC FIELD SAFETY LEVELS

This chapter deals with the risks on patients and personnel in the treatment room from high levels of R.F. electromagnetic fields created by the magnetic induction system. First, the effect of strong R.F. fields on patients is described in terms of direct heating of the tissue and in terms of the influence on the patient's nervous system. Second, the exposure of personnel to electromagnetic fields during treatment is presented together with recommendations to avoid any harmful consequences.

1. Risk to Patients

Risks to patients are considered from two different perspectives. The first is the possibility of direct tissue heating because of the strong R.F. fields and the other is the possibility of direct sensing of the electromagnetic field by the patient's nervous system.

The possibility of direct heating of the tissue by electromagnetic field is negligible. Stauffer et al[18] demonstrated that the power absorbed per unit volume from the 100 kHz field directly by the tissue is more than four orders of magnitude below that at 13.56 MHz which is

frequently used for inducing hyperthermia. The generator used in heating ferromagnetic seeds has a maximum power output of 8000 watts which is only one order of magnitude greater than the power used for direct tissue hyperthermia at 13.56 MHz. Therefore, 100 kHz fields pose no risk of extraneous tissue heating.

On the other hand, the possibility of risk from direct sensing of the R.F. field up to 60 kHz by the nervous system has been discussed by Borelli, Luderer and Panzarino[23] in relation to the use of hysteresis heating of ferrous fluids as a mean of inducing hyperthermia. They show that the field strength required for any sensing are of the order of 10,000 to 30,000 A/m which are one order of magnitude greater than those produced in the center of the coils used here. Therefore little risk arises from this effect.

2. Risk to treatment personnel

The American National Standards institute (ANSI) has published recommendations concerning safety levels with respect to human exposure to electromagnetic fields in the frequency range from 300 kHz to 100 GHz[11]. The ANSI radio-frequency guides (RFPG) are intended to apply to both occupational and nonoccupational exposure, but not to exposures of patients for medical purposes. These guides

specify maximum allowable levels as a function of frequency in terms of mean squared electrical and magnetic fields, E and H, respectively. To determine adherence to this RFPG, the square of the magnetic field strength should be averaged over any 0.1 hour period with all measurements to be made at a distance 5 cm or greater from any object. This is based on the presumption that the only harmful effect is that of tissue heating. The ANSI C95.1-1982 RFPG gives a limit of 1.6 A/m at 300 kHz. If we assume that the absorption efficiency of the field drops with the square of the frequency[12], then a safe level would be set at about 15 A/m. This value is observed at a distance of about 1 m from the C-coil and less for the other two coils. However, the International Non-Ionizing Radiation Committee of the International Radiation Protection Association (IRPA/INIRC) has published interim guidelines on limits of exposure to R.F. fields down to the 100 kHz frequency range[19] and set it at 0.51 A/m for the occupational exposure. This value of magnetic field strength is met at 4.7 m from the C-coil based on calculation on the 2 turn assumption at 7000 W of input power. In the clinical situation, field levels conforming to the IRPA/INIRC are therefore present only in the corners of the treatment room. Hence all personnel taking part in the therapy must remain in the corners of the room whenever the power is on. The treatment room is

shielded and therefore no restrictions apply to personnel outside.

On the other hand, the IRPA/INIRC have interim guidelines for limits of occupational exposure to electric fields down to the 100 kHz frequency[19], the value is set at 194 V/m. A mapping of the E field in the treatment room shows that levels conforming to the set limit are present at 1.5 m from the matching network. Note that the more stringent H field limits keep the personnel in the room at 4.7 m from the coil, which is effectively the corners.

CHAPTER 7

PERMEABILITY MEASUREMENT

The ferromagnetic seeds used for hyperthermia treatment are developed by Jong Sheng Chen at the University of Arizona and made of a Ni-Si alloy. Their magnetic properties allow for heating by magnetic induction and subsequently the heating of the surrounding tissue by heat conduction. The seed temperature is self regulating near (but slightly below) its Curie point because the material passes through ferromagnetic to paramagnetic phase transition as it approaches its Curie temperature and hence its ability to absorb power drops dramatically. The specific Curie temperature and transition range of a given seed depend upon its specific composition and upon the processing. Desired Curie temperatures are in the range from 50 to 70 $^{\circ}$C. The choice of a specific Curie point for the seeds to be used in a treatment depends on the blood flow in the implant. A low blood flow requires low temperature seeds for a successful and safe treatment, while for a high blood flow, up to 70 $^{\circ}$C seeds are used to assure the success of the treatment without excessively heating normal tissues.

Unfortunately, the specific magnetic properties of the seeds are difficult to control during manufacturing.

This makes seed reproducibility difficult to achieve. Since the performance of the seed must be known before it can be used in a treatment, it becomes necessary to measure the relative magnetic permeability as a function of temperature for each seed.

A preliminary system for that purpose was completed by Judith Kinney in the Department of Radiation Oncology[15]. The old system was manually operated and could only test one seed at a time. The operator monitored the temperature of the system while recording the results of the test.

The new system presented here is built on the same principle but can test up to 9 seeds at a time and is computer controlled.

1. Permeability Measuring System Overview

The permeability measuring system consists of a signal generator/amplifier, a long primary coil, nine short secondary pick up coils, a heated circulating water system, and a data acquisition and processing system. The entire set up is represented in Figure 25.

An R.F. sine wave with 100 kHz frequency is generated by the HP 3325A signal generator then amplified using an ENI 1140LA power amplifier. The amplified signal goes through a matching network to the primary coil. The

Permeability Measuring System
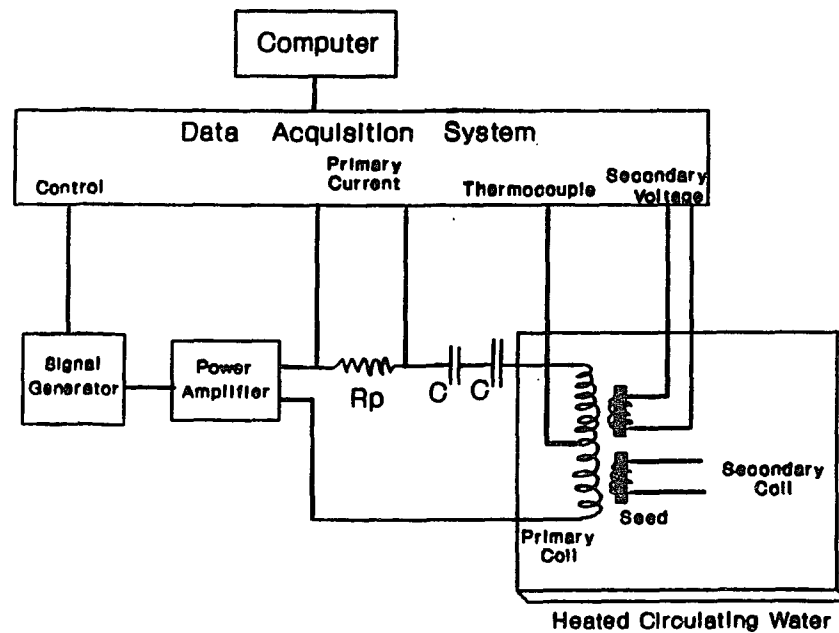
Figure 25. Overview of the experimental permeability measuring setup.

matching network consists of a resistor Rp and capacitors in series. The primary coil is a 250 turns copper wire wound around a glass tube 30 cm in length and 4 cm in diameter. Circulating water is heated on a hot plate before going through the glass tube. Immersed in the water, and inside the uniform field region of the primary coil, are nine secondary coils each with 10 turns wound around a small sample holder. Two T-type thermocouples are used for water temperature measurement. An HP 9836 computer using software written as part of this project controls the power output of the R.F. amplifier and its frequency by controlling the output of the signal generator. A flow chart of the acquisition part of the program is given in Figure 26. It was designed to record and display in real time the voltages appearing on the nine secondary coils and the temperature as the latter is slowly increased from 20 to about 80 °C. The current flowing through the primary coil is also recorded by measuring the voltage drop across Rp. The secondary voltage data are normalized to a primary current level which renders a 1 V signal across the primary current resistor, Rp (Figure 25). Thus, the properties of each seed can be directly compared. A typical output is shown in figure 27. The raw data consist of the values for the primary voltage and secondary voltages on each pick up coil along with their associated time and temperature readings.

Flowchart of Acquisition Program
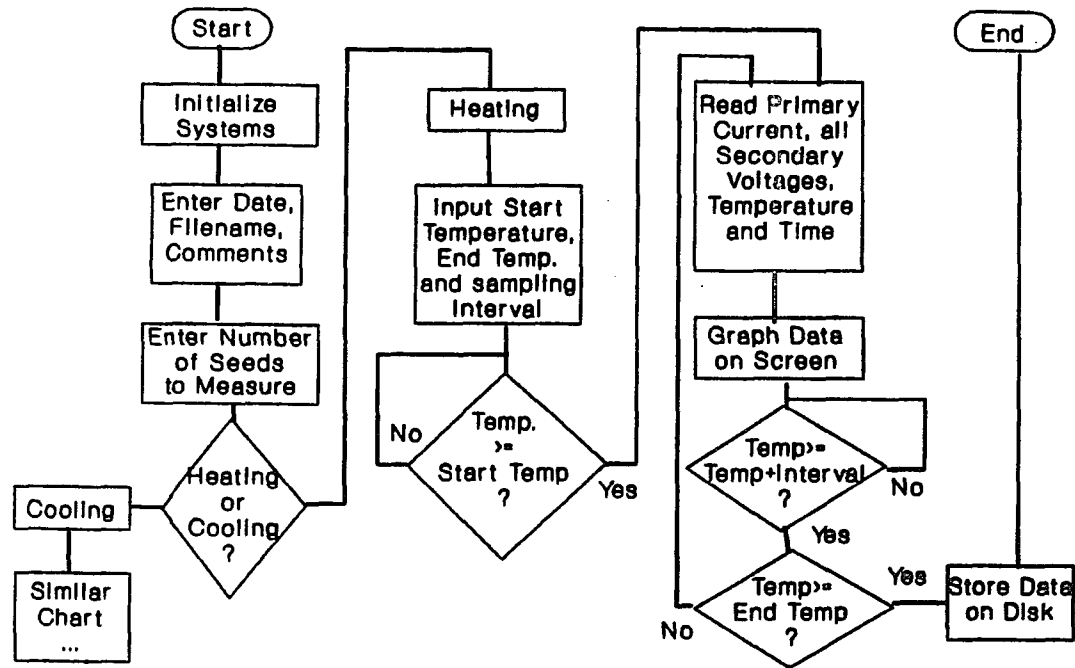
Figure 26. Flowchart of the data acquisition part of the software for the permeability measurement system.

Permeability of Ferromagnetic Seeds

Power Absorbed
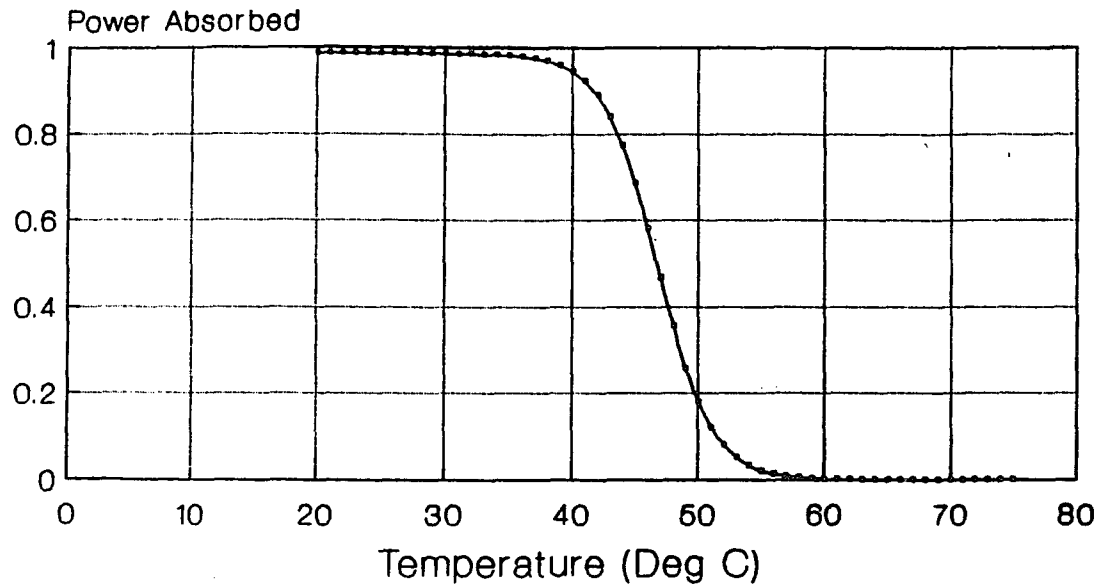
Temperature (Deg C)

Figure 27. Typical relative normalized power absorbed versus temperature for a ferromagnetic seed as recorded using the setup of Figure 25.

2. Principle of Operation

The principle of operation of the permeability
measuring system is as follows: The high current provided by
the power amplifier to the primary coil creates a magnetic
field by Ampere's law. This magnetic field is picked up by
the secondary coils sitting in the center of the primary.
The magnetic flux through in the secondary coils depends on
the permeability of the material present in the secondary
coils. The sinusoidal flux induces a voltage across the
terminals of the secondary coils by Faraday's law. As the
circulating water flowing in the coils heat the
ferromagnetic seeds in the secondary coil, their temperature
starts approaching their Curie point. At this time, their
permeability starts to drop decreasing the flux through the
secondary coils. As a result, the voltages induced in the
secondary coils diminishes.

3. Discussion

Numerous experiments were carried out to evaluate
the performance of the new permeability measuring device.
The results of the experiments are summarized in the
following.

1. When no material is present in any of the secondary
pick up coils, there is a finite voltage appearing on the
secondary terminals. The value of this voltage is about

0.014 volts and does not vary when the temperature is increased from 20 to 80 ^{o}C. This "empty coil", secondary voltage is a systematic correction and is substracted from the signal produced by a seed in that coil. As expected, it is equal to the value of the secondary voltage, with seed present in the coil, when the temperature is well over the Curie temperature.

2. When a seed is present in one secondary coil, no voltage over the noise level is observed in any other secondary coil. In other words, no detectable cross-talk occurs.

3. Introducing a seed made of 430 Stainless Steel material in a secondary coil produces a secondary voltage of 0.066 volts that does not vary with temperature (expected since the Curie point of 430 SS is about 660 ^{o}C).

4. The heating of a ferromagnetic seed is accomplished using circulating water heated slowly but continuously from 20 to 80 ^{o}C. Temperature and voltage measurements are taken at specific points during the heating process. Although temperature is increased slowly (at a rate of 1.2 degrees C per minute), thermal stability might not be present when data is taken because of the "ramp heating". A seed was tested first by heating then by cooling. The resulting curves of secondary voltages versus temperature superposed almost perfectly. This experiment shows that ramp heating in

this case works fine. However, for rapid heating or heating of very sharp transition seeds, the system currently used may lead to erroneous results. Hence a new temperature controller using a set temperature points for use with the permeability measuring system has been designed but not implemented yet.

5. Repeatability of the measurements for a given seed in a particular pick up coil are excellent. But a small difference between the pick up of any 2 different secondary coils is present. The variation is of the order of 0.01 volt or about 2%. This is due to the fact that the secondary coils are hand assembled and have inherent variations in size, shape and orientation with respect to the primary field. Nevertheless, the accuracy is well within our current requirements.

4. Initial Value for Permeability

The previous discussion provided a qualitative analysis giving relative permeability measurement. To determine the absolute value of the initial permeability of a ferromagnetic seed, we compute the sensitivity of the measurement system. Since the primary coil is a long solenoid, the value of the magnetic field can be computed. We use the assumption here that a 10 mm seed is long compared to the secondary pick up coil, about 1 mm, and

hence that we are sampling intrinsic material properties. This latter assumption has not been verified.

For a solenoid with N closely spaced turns and length l, from Ampere's law, the expression for the magnetic field B along its axis is:

$$B = \frac{\mu_o \cdot N \cdot I}{l}$$
Equation 2

Where μ_o is the permeability of free space and I is the primary current.

For a coil with a 4:1 length to diameter ratio, the field is nearly as large as that for an infinite coil[16]. Therefore, for the case of the primary coil,

$$Bo = \frac{\mu_o \cdot Np \cdot Ip \cdot \sin(wt)}{lp}$$

The presence of a high permeability ferromagnetic seed has a concentrating effect on the field. This results in the relation:

$$\frac{B_{seed}}{B_o} = \frac{\mu_{seed}}{\mu_o}$$

Where Bseed is the field subjected to the seed.

The flux through any secondary coil is given by:

$$\Phi = \iint Bseed.dA = \iint Bo.\frac{\mu_{seed}}{\mu_o} . dA \qquad \text{Equation 3}$$

$$\Phi = \mu_o.\frac{Np.Ip.\sin(wt)}{lp} .\frac{\mu_{seed}}{\mu_o} . \iint dA$$

At 100 kHz, the effective area of the seed is limited to the skin depth of the ferromagnetic material. The skin depth is approximated from the actual current distribution in a cross-section of a seed. Figure 7 shows such a distribution. By assuming that for $\delta << r$, where r is the radius of the seed, the total area enclosed by the curve is equal to the area of the rectangle at with a small side equal to δ . The skin depth is then defined as[17]

$$\delta = (\frac{2}{u.w.\sigma})^{1/2}$$

where σ is the electric conductivity of the seed. We can indeed make such approximation since a typical value of δ is about 0.1 mm. This value will be supported by measurements described later.

Then, the flux through the secondary coil becomes

$$\Phi = \frac{Np.Ip.\sin(wt)}{lp} . \mu_{seed} .(2.\pi .r. \delta)$$

where r is the radius of the seed.

From Lenz' law this flux induces an e.m.f. in the secondary coil with value

$$Es = - Ns \frac{d\Phi}{dt}$$

where Ns is the number of turns in the secondary coil. Then,

$$Es = \frac{- Ns.Np.Ip}{lp} . \mu_{seed} (2.\pi .r.\delta).\frac{d(sinwt)}{dt}$$

$$\Rightarrow \quad Es = - \frac{Ns.Np.Ip.\mu_{seed}.2.\pi .r. \delta}{lp} . w.cos(wt)$$

Finally, replacing δ by its value, we get

$$Es = - \frac{Ns.Np.Ip.2.\pi .r \left(\dfrac{2. \mu}{w. \sigma}\right)^{1/2}}{lp} . w.cos(wt)$$

By measuring the peak value of Es, we could retrieve Es(peak) in the expression

$$Es \ (peak) = \frac{Ns.Np.Ip.2.\pi .r. \left(\dfrac{2.\mu.w}{\sigma}\right)^{1/2}}{lp} \qquad \text{Equation 4}$$

solving for the permeability μ , we get

$$\mu = \frac{\sigma}{8.w} \cdot \left(\frac{Es \ (peak) \ . \ lp}{Ns.Np.Ip.\pi.r} \right)^2 \qquad \text{Equation 5}$$

This expression is a valid approximation at high permeability or at the initial permeability of the seed, before going through the Curie transition. The reason is that when the permeability decreases, the value of the skin depth approaches that of the radius of the implant and the implicit approximation $\delta \ll a$ breaks down.

CHAPTER 8

CONDUCTIVITY MEASUREMENT

So far we have measured two parameters affecting the power absorbed by a ferromagnetic seed, namely the strength of the magnetic field generated by the different induction coils and the permeability of the seeds. The third and final parameter is the electrical conductivity of the seeds. In this chapter, a device to measure the electrical conductivity is presented together with the measurement results.

1. Conductivity Measurement - Theory

In a cylindrical conductor of length l and cross sectional area A, the resistance is calculated from

$$R = (1/\sigma)(l/A)$$

where σ is the electrical conductivity.

Then, for the ferromagnetic seed, a measure of its resistance allows for a computation of the conductivity. We must however distinguish between two cases here, the DC case and the AC case. At DC, the effective area of the seed is r (total cross sectional area). But at AC, and because of the high permeability of the seed, the effective area is limited by the skin depth and is equal to $2\pi r.\delta$. Since

the permeability of the seed decreases with temperature, the skin depth increases until $\mu = \mu o$. The effective area is changing from a thin layer on the surface of the seed to the total cross sectional area. The result of that on the measured resistance is the following:

1. For DC fields, the resistance of the seed (Rdc) is constant and does not vary with temperature over the range of interest (20 to 80 degrees C).

2. For AC fields (100 kHz), the resistance of the seed (Rac) is increased due to the lower effective cross-sectional area since the currents are flowing near the surface. Rac decreases with the decrease of permeability until $\mu = \mu o$, this is when Rac becomes equal to Rdc.

The conductivity computation is straight forward for the DC case and is equal to

$$\sigma = (1/Rdc)(d/\pi r^2) \qquad \text{Equation 6}$$

where d is the length of the sample.

For the AC case, the conductivity (at low temperature, high permeability) is computed from

$$\sigma = (1/Rac)(d/2.\pi.r.\delta)$$

However,

$$\delta = \left(\frac{2}{w.\mu.\sigma}\right)^{1/2}$$

Then,

$$\sigma = \frac{1}{Rac} \cdot \frac{d}{2.\pi.r.\left(\frac{2}{w.\mu.\sigma}\right)^{1/2}}$$

$$\Rightarrow \quad \sigma = \frac{1}{4\pi} \cdot (f \cdot \mu) \cdot (\frac{d}{r})^2 \cdot \frac{1}{Rac^2} \qquad \text{Equation 7}$$

So knowing the conductivity of a seed from AC measurements at temperatures above the curie point or from DC measurements, we can retrieve the permeability from Equation 7. This equation is valid only at high value of permeability. As the temperature increases, and the permeability drops, the skin depth of the seed increases and the approximation for the effective area breaks down.

2. Experimental Set Up

In order to verify the theory, and to have a measurement of the resistance of the ferromagnetic seed, an experiment is conducted using a 4 terminal impedance measurement system. The set up is presented in Figure 28.

The apparatus is composed of a seed holding mechanism for 4-terminal impedance measurement, an HP 4277A LCZ meter, a heated circulating water system and a thermalert model TH6D thermometer that uses T-type thermocouples.

The holding mechanism attaches two spring loaded copper plates on the ends of a ferromagnetic seed passing a current through the specimen while two sharp ended probes pick up the complex voltage drop from the seed's body. The

Impedance measurement
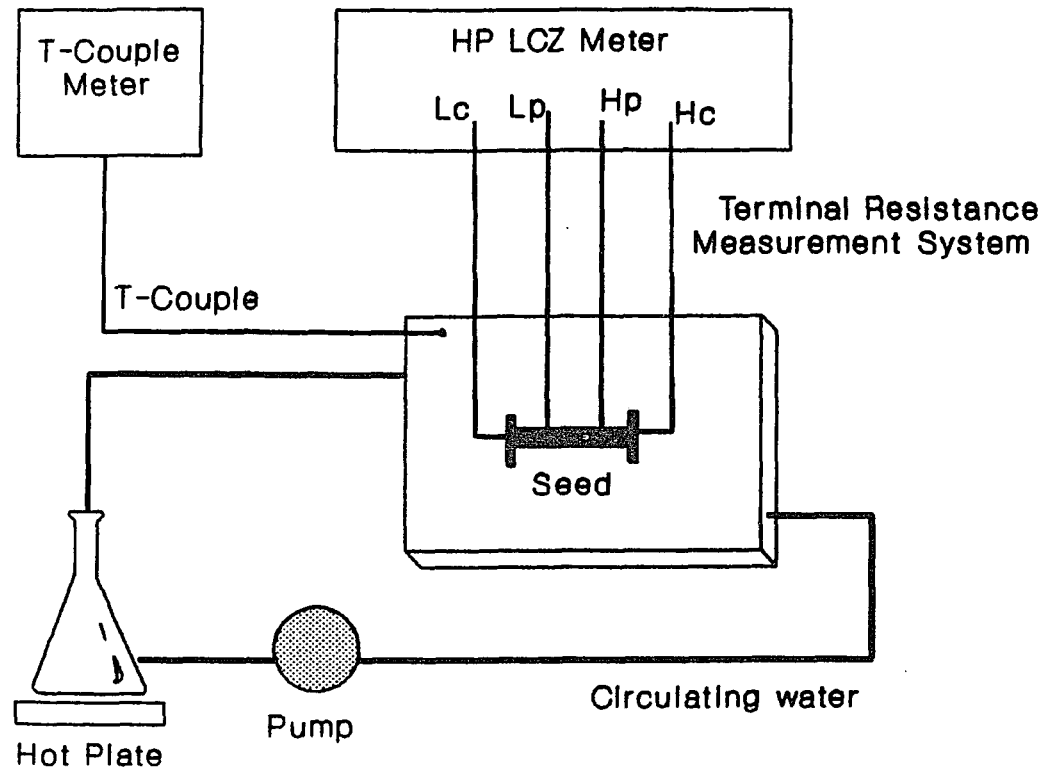
Figure 28. Experimental setup for the inductance and the resistance measurement of the ferromagnetic seed.

voltage probes have a fixed separation of 7.1 mm. The seed bathes in circulating water that is heated as a thermocouple monitors the temperature very close to the seed surface. The 4 lines (2 to feed the current and 2 to sense the potential drop) are directly connected to the HP vector impedance meter. The meter is operated at 100 kHz and displays the equivalent series resistance and the inductance of the specimen under test.

A copper seed with comparable dimensions to the ferromagnetic seeds was first inserted in the device and used for calibration. No deviation from zero ohms (less than 0.0001, the sensitivity of the meter) was observed for the copper as the temperature was increased to 70 °C.

When different ferromagnetic seeds were subjected to the same treatment, they all showed a sharp drop in both resistance and inductance around their curie points. A typical output is shown in Figure 29. ESR in the figure stands for Equivalent Series Resistance.

3. Discussion

By looking at the curves of seed temperature versus ESR we can notice the sharp drop in resistance around the curie point of the seed. This drop levels off at high temperatures suggesting that the skin depth has reached the total cross sectional area of the seed meaning that its

Inductance and ESR
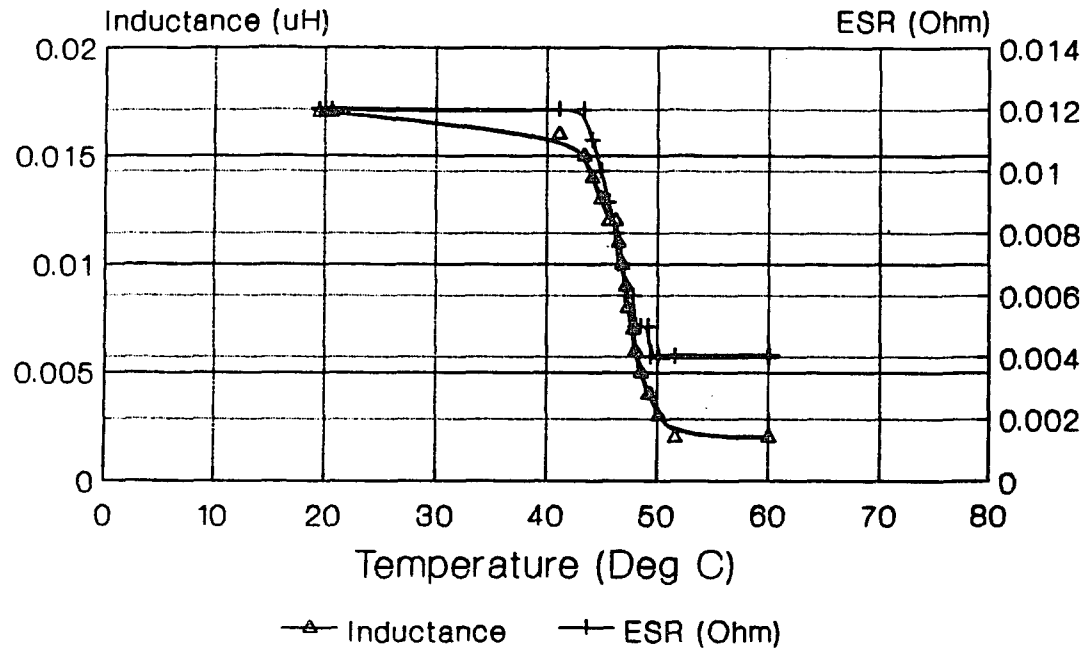
Figure 29. Typical inductance and equivalent series resistance versus temperature graph. Data recorded using the setup of Figure 28.

resistance is now Rdc. Indeed, 4-terminal resistance measurements were carried out using the same set up by with a DC Ohmmeter model HP 3456A, and showed the same value for Rdc.

The resistance curves could also be used to determine the curie point of the seeds and their transition ranges, just like the curves obtained from the permeability measuring device. However, the HP vector impedance meter can only measure one sample at a time and does not have the switching capabilities of the data acquisition system that can measure nine seeds or more simultaneously (by adding more secondary coils to the permeability measuring device, more seeds can be tested at the same time).

The permeability measuring device permitted the derivation of an equation for the absolute permeability of the seed (Equation 5). This equation shows the permeability as a function of conductivity. Equation 7 gives the same relation of conductivity as a function of the permeability as measured on the conductivity measuring device. Equations 5 and 7 are then the same equations.

To retrieve the value of permeability of a seed from either Equations 5 or 7, the value of the conductivity must be known from Equation 6.

4. Experimental Results

Three different batches of seeds (A, B, C) are selected and three seeds from each batch are tested. Seeds from a particular batch are supposed to have similar properties. Each seed is first tested on the permeability measuring device then on the conductivity measuring system. Their conductivity is computed from Equation 6 and shown in Table 4. Their permeability is calculated first from Equation 5 and shown in Table 5, then from Equation 7 and show in Table 6. The physical parameters used in the equations are:

Current flowing through the primary coil, $I_p = V_p/2$,

Angular frequency, $w = 2\pi.100\text{x}10^3$,

Length of primary coil, $l_p = 0.3$ m,

Number of turns in the primary coil, $N_p = 250$,

Number of turns in the secondary coil, $N_s = 10$,

Radius of the seeds, $r = 0.5\text{x}10^{-3}$ m,

Distance between the two voltage probes $d = 7.1\text{x}10^{-3}$ m.

We have presented two different methods to arrive at a value for the permeability of a ferromagnetic seed. Comparing the results from Table 5 and Table 6, we see a variation between 2 to 30 percent giving a root mean square deviation of +16.14 %.

Seed Type	R_{dc} (Ohm)	Conductivity* (S/m)
A1	0.004	2.26×10^6
A2	0.004	2.26×10^6
A3	0.004	2.26×10^6
B1	0.004	2.26×10^6
B2	0.004	2.26×10^6
B3	0.004	2.26×10^6
C1	0.004	2.26×10^6
C2	0.004	2.26×10^6
C3	0.004	2.26×10^6

* Calculated using equation 6

Table 4. Conductivity values of ferromagnetic seeds using measured values of the DC resistance.

Seed Type	V_p (V)	$I_p{=}V_p/2$ (A)	E_s(V)	Relative Perm.
A1	0.463	0.231	0.072	202
A2	0.463	0.231	0.072	202
A3	0.463	0.231	0.068	180
B1	0.463	0.231	0.082	262
B2	0.463	0.231	0.070	191
B3	0.463	0.231	0.064	160
C1	0.463	0.231	0.062	150
C2	0.463	0.231	0.068	180
C3	0.463	0.231	0.085	281

Table 5. Relative permeability of ferromagnetic seeds from measurements of primary current and secondary voltages using the permeability measuring system and Equation 5.

Seed Type	R_{ac} (Ohm)	Relative Permeability	% Difference*
A1	0.014	219	7.76
A2	0.015	252	19.84
A3	0.014	219	17.81
B1	0.016	287	8.71
B2	0.014	219	12.78
B3	0.014	219	26.94
C1	0.014	219	31.50
C2	0.014	219	17.81
C3	0.016	287	2.09

* Shows the % difference in relative permeability value between the permeability measurement and the AC resistance measurement.

Table 6. Relative permeability of ferromagnetic seeds from measurements of the AC resistance using the conductivity measuring system and Equation 7.

CHAPTER 9

HYSTERESIS MEASUREMENT

Previous work on seed efficiency and power absorption was carried out under the assumption that heating of the seed was caused by eddy currents flowing on the surface of the seed, neglecting any contribution from hysteresis heating[18]. In this chapter, a mathematical expression for the hysteresis losses is derived from an experimental set up, then measurement of a multiple of seeds is presented comparing hysteresis power loss to eddy current loss.

1. Experimental Set Up

The same set up used for the permeability measurement is used here (Figure 25) to demonstrate the hysteresis cycle and extact measurements of the power losses due to hysteresis. The voltage across Rp is fed to the X axis of an oscilloscope while a secondary coil voltage is applied to the Y axis. The shape of Figure 30 is then observed.

2. Theory

The area enclosed by the hysteresis loop represents

Hysteresis curve
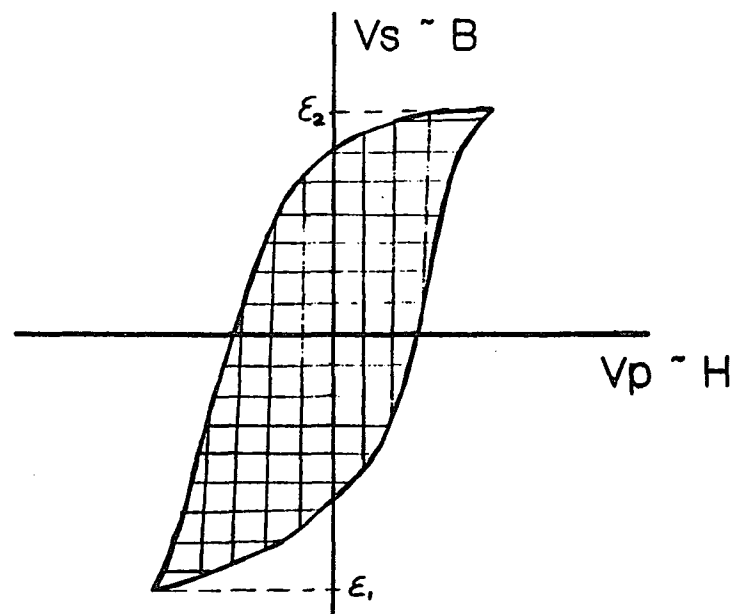
Figure 30. Hysteresis curve of a ferromagnetic seed as recorded on an oscilloscope from the setup of Figure 25.

energy dissipated as heat. This will become apparent in the following discussion.

When an alternating field of frequency f is applied to the ferromagnetic seed, the hysteresis power loss P_h in the seed is given by[13]

$$P_h = W_h \cdot f$$

Where W_h is the energy dissipated during each hysteresis cycle.

An expression for W_h will now be derived. Referring to Figure 30, if the current I is increased by an amount dI, the H field will increase by an amount dH and the B field by an amount dB. If this takes place in a time interval dt, then by Lenz' law an electromotive force

$$E = - N \frac{d\Phi}{dt}$$

will be induced in the windings tending to oppose the increase in current. The induced e.m.f. is opposite to the e.m.f. of the generator causing the increase of current. To increase I, the generator must furnish energy of amount

$$\triangle W = -E.I.dt = Np.Ip.d\Phi$$

We know that

$$d\Phi = Aeff.dB \qquad \qquad \text{Equation 9}$$

where Aeff is the effective area of the seed (limited by the skin depth).

The H field due to the current in the primary coil is given by

$$H = \frac{Np.Ip}{lp}$$ Equation 10

From Equations 9 and 10, $\triangle W$ becomes

$$\triangle W = lp.Aeff.H.dB$$
$$\Rightarrow \quad W = lp.Aeff \int_B H.dB$$ Equation 11

The area enclosed in figure 32 could now be seen as being effectively W.

An equation for the hysteresis power loses in terms of Vp (the voltage across the resistance in the primary coil circuit) and Es (the voltage appearing across any secondary coil) will now be derived.

From Equation 4, the B field in terms of Es is

$$B = \frac{\mu_o}{Ns.2.\pi.r \ (\frac{2\mu w}{\sigma})^{1/2}} \ . \ Es$$

Then, from Equation 11,

$$W_h = lp.2.\pi.r \oint (\frac{2}{\mu.w\sigma})^{1/2} \ \frac{Np.Vp}{lp.Rp} \ . \ [\frac{\mu_o}{Ns.2.\pi.r} \ (\frac{\sigma}{2.\mu.w})^{1/2}].dEs$$

$$\Rightarrow \quad W_h = \frac{Np}{Ns.Rp.w} \cdot \frac{\mu_o}{\mu} \oint_{\varepsilon_1}^{\varepsilon_2} Vp.dEs$$

Finally,

$$P_h = \frac{Np}{2.\pi.Ns.Rp} \cdot \frac{\mu_o}{\mu} \oint_{\varepsilon_1}^{\varepsilon_2} Vp.dEs \qquad \text{Equation 12}$$

μ here is the "effective alternating current permeability" which is an average ratio of B/H for the entire hysteresis loop.

The power lost in a ferromagnetic seed due to eddy currents was previously derived[18] and was found to be

$$P_e = \frac{\pi.r.ls}{(2)^{1/2}} \left(\frac{w.\mu}{\sigma}\right)^{1/2} .H_o^2$$

Where ls is the length of the seed and H_o is the applied magnetic field strength.

In the case of the set up of Figure 25, P_e will become

$$P_e = \frac{\pi.r.ls}{(2)^{1/2}} \left(\frac{w.\mu}{\sigma}\right)^{1/2}. \left(\frac{Np.Vp}{lp.Rp}\right)^2 \qquad \text{Equation 13}$$

3. Experimental Results

The same seeds used for the permeability and conductivity measurements were tested for hysteresis losses.

The experimental set up of Figure 23 is used to get

the results expressed in Table 7 for the hysteresis power losses. These results are based on calculations using Equation 12 and assuming that the relative permeability of the seeds is 200. The hysteresis losses are then compared to eddy current losses using Equation 13 and the data is given in Table 8.

Additional physical parameters used for these calculations are: Temperature = 25 °C (ambient temperature)

Np = 212   lp = 0.24 m

Ns = 10   ls = 10 x 10^{-3} m

Rp = 50 Ohm

r = 0.5 x 10^{-3} m

w = 2.π x 100 x 10^3 rps

μ = 200 x 4.π x 10^{-7} H/m

σ = 2.26 x 10^6 S/m

As an example, take seed A1, the area enclosed by the hysteresis cycle is about 17 squares as seen on an oscilloscope when the scale is at 5 V/division horizontal and 20 mV/division vertical. Therefore, the area enclosed by the hysteresis cycle is 5 V/div x 20 x 10^{-3} mV/div x 17 div^2 = 1.7 v^2

Replacing this value in Equation 12, we get

$$P_h = \frac{212}{2.\pi \times 10 \times 50} \times \frac{1}{200} \times 1.7 = 0.57 \times 10^{-3} \text{ Watt}$$

Seed Type	Area enclosed by hysteresis loop (V^2)	Hysteresis Power loss (W)
A1	1.7	0.57×10^{-3}
A2	1.8	0.61×10^{-3}
A3	1.8	0.61×10^{-3}
B1	1.8	0.61×10^{-3}
B2	1.7	0.57×10^{-3}
B3	1.8	0.61×10^{-3}
C1	1.7	0.57×10^{-3}
C2	1.7	0.57×10^{-3}
C3	1.7	0.57×10^{-3}

Table 7. Hysteresis power losses using the permeability measuring device and Equation 12 and assuming an average relative permeability of the seeds of 200.

Seed Type	Vp (V)	Eddy current losses(W)	Pe/Ph
A1	14	5.7×10^{-3}	10
A2	14	5.7×10^{-3}	9.3
A3	14	5.7×10^{-3}	9.3
B1	14	5.7×10^{-3}	9.3
B2	14	5.7×10^{-3}	10
B3	14	5.7×10^{-3}	9.3
C1	14	5.7×10^{-3}	10
C2	14	5.7×10^{-3}	10
C3	14	5.7×10^{-3}	10

Table 8. Eddy current power losses in ferromagnetic seeds using Equation 13. Also, ratio of Eddy current losses to hysteresis losses.

The primary voltage is measured and is found to be Vp = 14 V (across a 50 Ohm resistor). The eddy current losses are therefore from Equation 13

$$P_e = 5.7 \times 10^{-3} \text{ Watt}$$

The ratio of P_e to P_h is then

$$P_e/P_h = 10$$

This previous analysis shows that for practical purposes, the effect of hysteresis on heating the seeds can be ignored. However, for precise studies, hysteresis losses should be included.

CHAPTER 10

CONCLUSION

The ferromagnetic seed system as a mean of inducing hyperthermia has been used for the treatment of numerous cancer patients during the past two years. Results of these treatments show that the system can raise the temperature of a well localized volume of tissue to therapeutic levels. Even in high blood flow situations, such as brain implants, temperatures of over 42 °C were achieved and maintained throughout the prescribed period of time. It was found, as predicted, that once the applied power was sufficient to cause the seeds to attain their Curie point, large increases in power caused very little further heating. On some occasions, therapeutic temperatures were not reached in the first 10 minutes of the treatment. In these cases, the seeds were exchanged with higher Curie point seeds, and the treatment was successfully continued.

1. Quality Assurance Issues

Quality assurance for the system was performed on the magnetic induction device level and on the seed level.

On the coils and fields level, a magnetic field probe for frequencies around 100 kHz was built and used to

map the field in all space and for the three coils utilized with the system. Field levels produced by the three coils were found to be adequate for generating enough heat in the ferromagnetic seeds with no risk to the patients from direct tissue heating or from nervous system sensing. Treatment personnel present inside the shielded room are recommended to remain in the corners of the room whenever the power is on. Although electric fields produced by the magnetic induction system do not contribute appreciably to the seed heating, their measurements were carried out for safety reasons. The results showed that electric field levels require treatment personnel to be limited to 1.5 m away from the matching network and therefore the more stringent magnetic field requirements should be obeyed.

On the seeds level, an automated permeability measuring device was built and used to measure the relative permeability of the ferromagnetic seeds, their Curie temperature and the value of their initial permeability. A measurement of the electrical conductivity for the seeds was also performed as a mean to arrive at a value for the initial permeability. Variations between the two methods were between 2 to 30 % giving a root mean square deviation of +16.14 % for the conductivity measurement.

Analysis of the hysteresis losses in a seed proved that their contribution in seed heating was ten times lower

than losses due to eddy currents and therefore negligible.

2. Future Developments

Although the system performed well, there are still areas of optimization for ease of operation as well as for better clinical implementation. These include:

1. The magnetic induction system requires cooling water in the coil and the matching network. It is imperative that cold water flows in the system. A digital flow meter was built to monitor the flow in the silicone hoses between matching network and induction coil. The monitor measures the rotational frequency of a plastic wheel located inside the hose using an infrared transmitter/receiver pair and translate this information to a unit of flow. The flow meter still has to be adapted so that the readout is located outside the shielded room, where the operator controls the power. In case of low water flow, the magnetic induction system should not be turned on in order to assure the safety of the patients and treatment personnel.

2. A permanent temperature monitor of the circulating water also gives an additional safety item.

3. The cooling water reservoir and the power generator are

located in an attic located over the shielded room and the control room. A remote power button for the generator and a water level indicator for the cooling water would do without climbing to the attic for every treatment.

4. A new design for a coil holder would allow the orientation of a coil in all possible direction of implant. This would make the generated magnetic field more efficient in seed heating. Such holders should permit a low resistance electrical connection between the matching network and the coil and also the free flow of water through the electrical connection.

5. Another efficiency issue is the production of higher permeability ferromagnetic seed. This will allow the use of a smaller power generator and smaller induction coils and might even enable building a portable system that would not be limited by a shielded room.

3. Quality Assurance Procedures

Current pre-treatment quality assurance procedures includes the following:

1. Measurement of the relative permeability of every seed required for the treatment using the automated permeability measuring system.

2. Checking for all electrical connections in the magnetic induction system.

3. check for sufficient deionized water in the cooling system and check for correct flow.

4. Turning the power on and checking for proper matching between coil and power generator. This is done by fine tuning the generator's output frequency until the reflected power is minimized.

5. Frequency check inside the shielded room using a multiturn pick up coil connected to a hand held frequency meter.

6. Measurement of the magnetic field at the center of the coil at low power levels (200 to 1000 Watts) using the optically coupled magnetic field probe. The measured value should be compared to the reported value in this thesis.

7. Testing the system at high levels of power (7000 Watts) for few minutes and sensing any unusual increase in temperature in the rubber cooling water hoses.

8. Holding a ribbon of seeds close to the center of the coil and checking for appreciable heating at moderate power levels (3000 to 5000 Watts).

9. Checking of all thermometry probes at high level of power for correct readings free of artifacts.

10. Running the treatment data acquisition system and checking for correct temperature and power level recording.

During the treatment, quality assurance issues include:

1. Measurement of the frequency at 10 minutes interval using the hand held frequency meter.

2. Frequent visual check of the cooling water flow and sensing the rubber hoses for any unusual increase in water temperature.

APPENDIX A

TEMPERATURE COMPENSATION

Temperature compensation in semiconductor junctions can be achieved by using the linearizing thermistor network as presented by Jaffe[7].

The typical resistance-versus-temperature curve for a thermistor is nonlinear (Figure 31). However, the element to be compensated for is a silicon junction whose AC small signal resistance is

$$Rac = \frac{n.k.T}{q.I} + Rbulk$$

where

k = Boltzman's constant,

T = temperature in degrees Kelvin,

q = electron charge,

I = DC bias current,

Rbulk = bulk resistance, and

n = a constant with value between 1 and 2.

Since this function is non-linear, simply placing a thermistor with a negative temperature coefficient in series with the junction will not properly compensate the network. Thus the thermistor must be "linearized". In addition, its

Typical Thermistor Curve
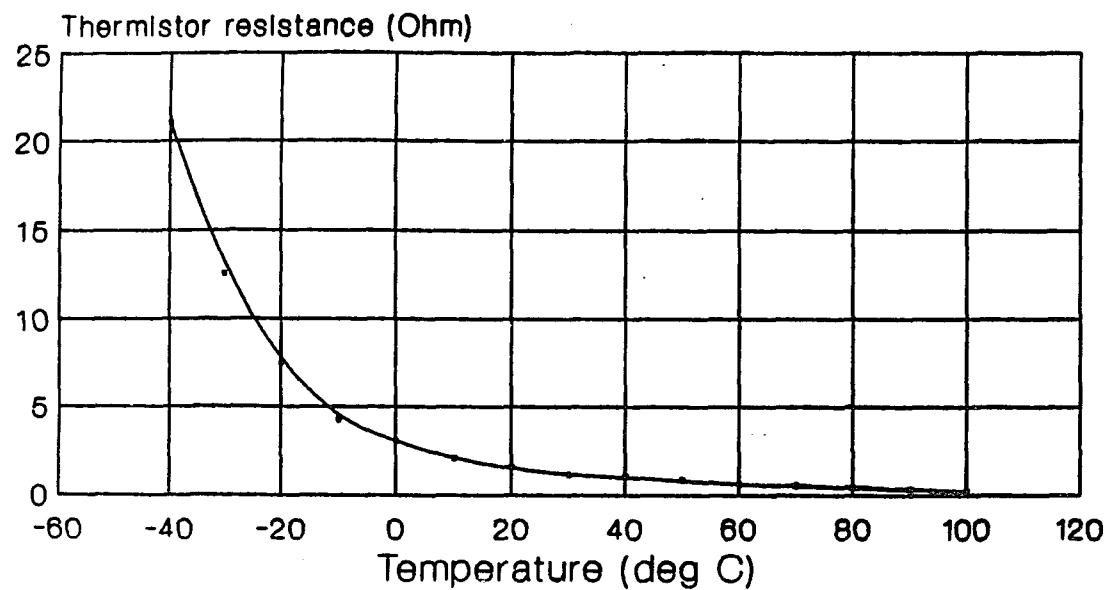
Thermistor resistance (Ohm)

Figure 31. Typical thermistor curve showing the thermistor resistance versus temperature.

change in resistance versus temperature must be determined, as well as the absolute resistance for a given temperature.

The temperature coefficients of the junction is first found by referring to the graph in Figure 6. The percent change in the output is graphically determined by:

$$\% \text{ change} = (\frac{1}{Vo}) \cdot (\frac{\Delta Vo}{\Delta T}) \qquad @Va=1.5 \text{ volts rms}$$

Vo = the average output between temperatures T1 and T2

Δ Vo = output voltage difference

Δ T = temperature interval T1-T2

Va = applied loop voltage parameter

An average temperature coefficient over the region of interest is obtained. The value of -1.05 %/^{o}C is necessary for compensation over a temperature range of 25 to 50 ^{o}C.

Temperature compensation is accomplished with negative temperature coefficient thermistor properly linearized. The linearization circuit is shown schematically in Figure 32. From this circuit, Jaffe uses the "equal slopes" technique to get a value he denotes S and is given by:

$$S = \frac{T2 \ [r(T1)]^{1/2} \ - \ T1 \ [r(T2)]^{1/2}}{T1.r(T1).[r(T2)]^{1/2} - \ T2.r(T2).[r(T1)]^{1/2}}$$

where

T1 = lower temperature limit in degrees K,

T2 = upper temperature limit in degrees K, and

r(T) = normalized thermistor resistance at temperature T.

From S, equations for the resistor in parallel with the thermistor (Rp) and for the series resistor (Rs) are obtained as follows:

$$Rp = \{ \ S \ r(T1).r(T2) \ + \ S[r(T1)+r(T2)+1] \} \ \frac{\Delta \ (T2-T1)}{S[r(T2)-r(T1)]}$$

$$Rs = Rd - \frac{R(To).Rp}{R(To)+Rp}$$

where

R(To) = thermistor value to select at 25 degrees C,

Rd = desired total circuit resistance

$\Delta = \Delta R / \Delta t$ needed for proper compensation.

Using these equations and data from Thermometrics thermistor sensor handbook[8], to compensate an LED with a temperature coefficient of -0.0105, using a -3.9%/^{O}C

Linearization Circuit

Thermistor

Rs

Rp
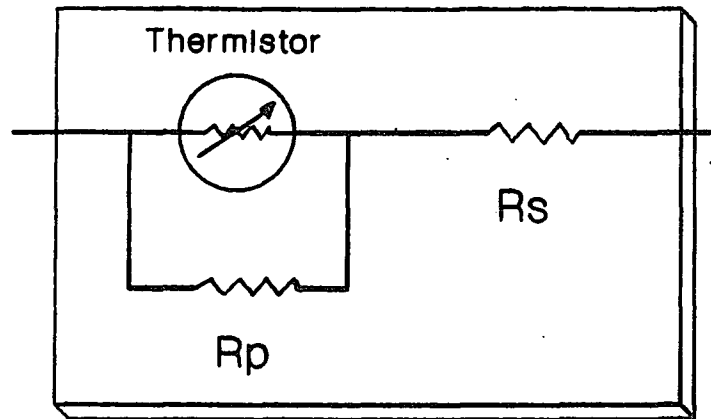
Figure 32. Jaffe temperature compensation circuit.

thermistor,the values of the corresponding components are:

      Rp = 5.86 KOhm

      Rs = 3.45 KOhm

      Rth= 15.7 KOhm @ 25 ^{o}C

The compensated network showed an excellent temperature independence (Figure 6).

LIST OF REFERENCES

1. Buechler, Dale Norman."Magnetic Induction Heating of Ferromagnetic Implants for Hyperthermic Treatment of Cancer." Thesis submitted to the faculty of the Department of Electrical and Computer Engineering. University of Arizona, Tucson, Arizona 1986.

2. Cetas, T.C., Roemer, R.B., "Status and future developments in the physical aspects of hyperthermia." Cancer Research (Suppl.), Vol. 44, pp. 4894s-4901s, Oct. 1984.

3. Gross, Eugene Joseph, "Optical Magnetic Field Probe with Light Emitting Diode Sensor." Thesis submitted to the faculty of the Department of Electrical and Computer Engineering. University of Arizona, Tucson, Arizona 1986.

4. Henrichsen, K.W. "Large Scale Magnetic Field Measurements and Mapping", 8th International Conference on Magnetic Technology, Grenoble 1984.

5. Nahman, N.S., Kanda, M., Larsen, E.B. and Cranford, M.L., "Methodology for Standard Electromagnetic Field Measurements", IEEE Transactions on Instrumentation and Measurement, IM-34, pp.490-503, 1985.

6. Stanley Semiconductor Technical Notes. Catalog No. E-186-1-4.

7. Jaffe, Stan, "Temperature Compensation Using Thermistors", Microwaves and RF, Vol. 23, No. 4, pp.101-104, April 1984.

8. Thermistor Sensor Handbook, Thermometrics, Inc. 808 US Highway #1, Edison, New Jersey, 08817, 1986.

9. Amphenol, "Fiber Optics Designer's Handbook", Catalog No. f122-00077, September 1982.

10. Halliday, D. and Resnick, R., Physics Part 2, Fundamentals of Physics, 3rd edition, John Wiley and Sons, Inc., New York, 1978.

11. "American National Standard Safety Levels with respect to Human Exposure to Radio Frequency Electromagnetic Fields, 300KHz to 100GHz". ANSI C95.1 - 1982. Institute of Electrical and Electrononis Engineers, 1982.

12. Stauffer, P.R., Cetas, T.C., Fletcher, A.M., et al. "Observations on the Use of Ferromagnetic Implants for Inducing Hyperthermia", IEEE Transactions on Biomedical Engineering, Vol 31, pp. 76-90, January 1984.

13. Plonus, Martin A., "Applied Electromagnetics", McGraw-Hill Book Company, New York, 1978.

14. Chen, J.S. et al, "Development of Ni-4 % Si Thermoseeds for Hyperthermia Cancer Treatment." Journal of Biomedical Materials Research, Vol. 22, pp.303-319, 1988.

15. Kinney, Judith B. "Design and Construction of a Device to Measure Permeability of Ferromagnetic Seeds." Technical Report, May 1985.

16. Plonus, Martin A., "Applied Electromagnetics", McGraw-Hill Book Company, New York, 1978.

17. Corson, Dale R., Lorrain, Paul, "Introduction to Electromagnetic Fields and Waves", W. H. Freeman and Company, 1962.

18. Stauffer, Paul R., Cetas, Thomas C., Jones, Roger C., "Magnetic Induction Heating of Ferromagnetic Implants for Inducing Localized Hyperthermia in Deep Seated Tumors." IEEE Transactions on Biomedical Engineering, Vol. BME-31, No. 2, February 1984, Page 235.

19. International Non-Ionizing Radiation Committee of the International Radiation Protection Association, "Interim Guidelines on Limits of Exposure to Radiofrequency

Electromagnetic Fields in the Frequency Range from 100 KHz to 300 GHz." Health Physics,

20. Haider, S.A. "Ferromagnetic Implants in Hyperthermia: an Analytical, Numerical and Experimental Study." Thesis submitted to The Department of Electrical and Computer Engineering at The University of Arizona, December 1988.

21. Grover, Frederick W. "Inductance Calculations", Special Edition prepared for Instrument Society of America. Dover Publications, New York, N.Y. 1973.

22. Manning, M.R., Cetas, T.C., Miller, R.C., Oleson, J.R., Connors, W.G. and Gerner, E.W "Clinical Hyperthermia: Results of a Phase I Clinical Trial Employing Hyperthermia Alone or in Combination with External Beam or Interstitial Radiotherapy", Cancer, Vol.49, pp. 205-216 (1982).